DOT/FAA/AR-99/8,IV

Office of Aviation Research
Washington, D.C. 20591

Improved Barriers to Turbine Engine Fragments: Interim Report IV

June 2002

Interim Report

This document is available to the U.S. public through the National Technical Information Service (NTIS), Springfield, Virginia 22161

U.S. Department of Transportation
Federal Aviation Administration

20020806 090

NOTICE

Technical Report Documentation Page

1. Report No. DOT/FAA/AR-99/8,IV	2. Government Accession No.	3. Recipient's Catalog No.
4. Title and Subtitle IMPROVED BARRIERS TO TURBINE ENGINE FRAGMENTS: INTERIM REPORT IV		5. Report Date June 2002
		6. Performing Organization Code
7. Author(s) Donald A. Shockey, David C. Erlich, Jeffrey W. Simons, and Hyung-Seop Shin		8. Performing Organization Report No.
9. Performing Organization Name and Address SRI International 333 Ravenswood Avenue Menlo Park, CA 94025-3493		10. Work Unit No. (TRAIS)
		11. Contract or Grant No. 95-G-010
12. Sponsoring Agency Name and Address U.S. Department of Transportation Federal Aviation Administration Office of Aviation Research Washington, DC 20591		13. Type of Report and Period Covered Interim Report
		14. Sponsoring Agency Code ANE-100, ANM-100
15. Supplementary Notes The FAA William J. Hughes Technical Center COTRs: William Emmerling and Donald Altobelli.		

16. Abstract

This interim technical report describes the progress made during year 3 of SRI International's Phase II effort to develop a computational capability for designing lightweight fragment barriers for commercial aircraft. Fabrics of high-strength polymers have been shown to be excellent candidates for these barriers.

A series of large-scale fragment impact tests was performed at SRI's remote test site to characterize the resistance of full-scale fabric barriers to realistic fragment impact and provide data for model calibration and verification. These tests have demonstrated the importance of allowing material failure to occur near the held corners of a fabric barrier, but not allowing the corner to detach from the fuselage frame. In addition, SRI designed and implemented laboratory tests to characterize the cut resistance of the fabric yarns to sharp blades. Results show a strong effect of the slicing angle upon the energy absorbed during yarn failure.

Simulations using the detailed computational fabric model showed the effectiveness of holding the fabric at the corners. A time-efficient, user-friendly design model for fabric barriers is being developed. The model, previously calibrated against small-scale gas gun tests, was used to simulate the large-scale fabric impact tests. The results of the simulations showed that the current model is stiffer and stronger than the measured response of the fabric.

In a continuing effort to keep the civil aircraft community informed, SRI hosted the Fourth Federal Aviation Administration Workshop on Uncontained Engine Debris, updated its Aircraft Engine Fragment Barriers web site to include an overview of all work performed to date, and prepared several papers for submission to technical journals and symposia.

17. Key Words Aircraft engine fragments, Fragment barriers, PBO armor, Zylon		18. Distribution Statement This document is available to the public through the National Technical Information Service (NTIS), Springfield, Virginia 22161.	
19. Security Classif. (of this report) Unclassified	20. Security Classif. (of this page) Unclassified	21. No. of Pages 60	22. Price

Form DOT F1700.7 (8-72)   Reproduction of completed page authorized

ACKNOWLEDGMENTS

TABLE OF CONTENTS

LIST OF FIGURES

LIST OF TABLES

EXECUTIVE SUMMARY

This interim technical report describes the progress made during year 3 of the SRI International Phase II effort to develop a computational capability for designing lightweight fragment barriers for commercial aircraft. Fabrics of high-strength polymers have proven to be excellent candidates for these barriers.

A series of large-scale fragment impact tests was performed at SRI's remote test site to characterize the resistance of full-scale fabric barriers to realistic fragment impact and provide data for model calibration and verification. These tests have demonstrated the importance of allowing material failure to occur near the held corners of a fabric barrier, but not allowing the corner to detach from the fuselage frame. In addition, SRI designed and implemented laboratory tests to characterize the cut resistance of the fabric yarns to sharp blades. Results show a strong effect of the slicing angle upon the energy absorbed during yarn failure.

Simulations using the detailed computational fabric model showed the effectiveness of holding the fabric at the corners. A time-efficient, user-friendly design model for fabric barriers is being developed. The model, previously calibrated against small-scale gas gun tests, was used to simulate the large-scale fabric impact tests. The results of the simulations showed that the current model is stiffer and stronger than the measured response of the fabric.

INTRODUCTION AND BACKGROUND

Over the years, several civil aircraft accidents with catastrophic consequences have occurred when fragments from in-flight engine failures damaged critical aircraft components. To reduce the probability of catastrophic consequences in future failures, the Federal Aviation Administration (FAA) established the Aircraft Catastrophic Failure Prevention Research (ACFPR) Program [1] to develop and apply advanced technologies and methods for assessing, preventing, or mitigating the effect of such failures. In support of the ACFPR objective, SRI International is conducting research aimed at developing lightweight barrier systems for turbine engine fragments.

In Phase I of this program, SRI reviewed the rich body of armor technology documentation held by the Department of Defense to identify concepts, materials, and armor designs that could lead to practical barriers to engine fragments on commercial aircraft [2]. Because of their low density and high strength, highly ordered, highly crystalline, high-molecular-weight polymers were identified as the advanced materials holding greatest promise for engine fragment barriers on aircraft. Specifically, fabrics of certain aramids (Kevlar and Twaron), polyethylenes (Spectra and Dyneema), and polybenzobisoxazole (PBO, Zylon) appeared able to provide a useful measure of ballistic protection in the most weight-efficient manner. Furthermore, some of these materials appear to have sufficient flame resistance, water absorption resistance, and thermal and acoustic insulation properties to serve as building blocks for barriers.

Phase II is a combined experimental research and computational modeling program to demonstrate and characterize the ballistic properties of these high-strength fabrics, and develop a computational capability for designing the barriers. During the first 2 years of the Phase II program, SRI conducted small-scale impact tests at its remote test site, as well as full-scale fuselage impact experiments at Naval Air Warfare Center (NAWC), China Lake, using real fragments or fragment-simulating projectiles. These tests confirmed that lightweight barriers made of a few plies of these fabrics can absorb a substantial amount of fragment energy. SRI determined how the ballistic effectiveness of the fabric varied as a result of changes in the number of fabric plies, boundary conditions (how the fabric was gripped), and fragment sharpness.

To assist in model development, SRI performed quasi-static penetration tests with a tensile machine in conjunction with an audio-video camera to elucidate the phenomenology and evolution of fabric failure. Three different fabric failure mechanisms were observed, and the effects of multiple-fabric plies and gripping geometry were investigated. Tensile and friction properties of the fabric yarns were measured at several strain rates.

Computational models were developed at two different levels of material detail to facilitate design of barrier structures and assist in their evaluation. The detailed model treats individual yarns of the fabric explicitly, accounting for yarn geometry, properties, interactions with each other, and failure mechanisms. This model, implemented with brick elements in the LS-DYNA3D finite element code, was used to simulate ballistic experiments and compute the failure behavior of yarns and fabrics under impact scenarios. Fragment barriers were designed

using the insights gained from the simulations. The barriers were constructed, and their performance was evaluated in full-scale fragment impact experiments on a fuselage.

In the design model, the fabric was modeled with shell elements, which decreases the computation time significantly. This model was also used to simulate the fragment impact tests, and is intended for use by aeronautical engineers in designing fragment barriers.

At the conclusion of this program, a computational model and information on advanced materials that will enable airframers to design and evaluate lightweight engine fragment barriers will be developed. An important direct result of this effort will be practical fragment barriers that could be implemented on commercial aircraft.

This is a report of the progress made during calendar year 2000. The first section describes the large-scale impact tests on the fabric barriers performed both at NAWC-China Lake and at SRI's remote test site. The second section describes progress on the computational model development. The third section discusses technology transfer. The final section outlines plans for calendar year 2001. The work on the resistance of yarns is described in appendix A.

LARGE-SCALE IMPACT TESTING OF FABRIC BARRIERS

Large-scale impact tests were performed using both the NAWC 12-in.-bore gas gun at China Lake and the SRI 6-in.-bore gas gun to examine the effectiveness of the fabric barriers to realistic fragment impact scenarios. These tests involved actual fan or compressor blade fragments, weighing between 166 and 597 g (0.37 to 1.32 lb), and traveling at velocities up to 271 m/s (890 f/s), in the range of expected velocities for uncontained fragments.

FUSELAGE IMPACT TESTS AT NAWC-CHINA LAKE.

In October 1999, SRI International, in conjunction with the NAWC, performed a second series of full-scale fragment impact tests on a commercial transport aircraft fuselage section at China Lake, CA. The principal goals for this series were to (1) test the effectiveness of the fabric barriers against larger, more energetic engine fragments (in particular the type of fragments identified by analysis in the large engine debris report [3]) and (2) investigate the effect of various barrier attachment schemes on the ballistic capability. Last year SRI presented a preliminary report [4] that included a detailed description of the experimental procedure and the test matrix and a qualitative description of the test results. However, the analysis of the tests, including a determination by NAWC of the impactor (projectile) velocities and orientations from the high-speed movies, were not complete at that time. A review of the test setup and matrix is given below, along with the final test results.

TEST SETUP. The relevant test parameters are shown in table 1, including the mass and dimensions of the fragment impactor, the materials, dimensions, areal densities, locations, and attachment methods for the fabric barriers.

TABLE 1. SRI FUSELAGE IMPACT TESTS AT NAWC-CHINA LAKE (OCTOBER 1999)—TEST MATRIX AND RESULTS

Test No. CL-	Material[d]	Mesh	Plies	Areal Density (g/cm² / lb/ft²)	Width (cm / in.)	Height (cm / in.)	Total Area (m² / ft²)	Fabric Mass (g / lb)	Method of Attachment[e]	Sections below Window	Al. Skin Thickness (cm / in.)	Fragment Mass (g / lb)	Th. (cm / in.)	W. (cm / in.)	L. (cm / in.)	Roll (°)	Pitch (°)	Yaw (°)	Obliquity (°)	Velocity (m/s / f/s)	Residual K.E. (kJ / kft-lb)	Residual Velocity (m/s / f/s)	K.E. Lost (kJ / kft-lb)	Absorbed Fuselage Structure (kJ / kft-lb)	Absorbed Fabric Barrier (kJ / kft-lb)	SEA[c] (kJ g/cm² / kft-lb lb/ft²)
18	Zy	35	3	0.047 / 0.097	82.6 / 32.5	62.2 / 24.5	1.5 / 16.6	166 / 0.37	G/P	2nd	0.165 / 0.065	166 / 0.37	0.55 / 0.22	7.6 / 3.0	10.2 / 4.0	-19	-6	51	0	271 / 890	6.1 / 4.5	134 / 439	4.62 / 3.41	1.71 / 1.26	2.92 / 2.15	61.5 / 22.2
19	Zy	35	3	0.047 / 0.097	82.6 / 32.5	62.2 / 24.5	1.5 / 16.6	166 / 0.37	G/P	2nd	0.170 / 0.067	166 / 0.37	0.55 / 0.22	7.6 / 3.0	10.2 / 4.0	-26	-34	55	0	239 / 785	4.8 / 3.5	0 / 0	4.75 / 3.51	1.55 / 1.14	3.21 / 2.36	>68 / >24
20	Kev	32	3	0.034 / 0.069	82.6 / 32.5	62.2 / 24.5	1.5 / 16.6	166 / 0.37	G/P	2nd	0.160 / 0.063	181 / 0.40	0.64 / 0.25	7.6 / 3.0	10.2 / 4.0	-12	-16	-87	0	223 / 733	4.5 / 3.3	0 / 0	4.52 / 3.33	1.43 / 1.06	3.09 / 2.28	>91 / >33
21	Spec	32	3	0.032 / 0.066	82.6 / 32.5	62.2 / 24.5	1.5 / 16.6	166 / 0.37	G/P	2nd	0.259 / 0.102	181 / 0.40	0.64 / 0.25	7.6 / 3.0	10.2 / 4.0	13	22	18	0	240 / 788	5.2 / 3.9	0 / 0	5.22 / 3.85	1.29 / 0.95	3.93 / 2.90	>121 / >44
22	Zy	35	6	0.095 / 0.194	211 / 83.0	62.2 / 24.5	7.9 / 84.7	850 / 1.87	P	2nd & 3rd	0.241 / 0.095	597 / 1.32	0.84 / 0.33	14.0 / 5.5	17.8 / 7.0	27	10	-22	0	246 / 808	18.1 / 13.4	174 / 570	9.09 / 6.71	2.85 / 2.10	6.24 / 4.61	65.9 / 23.7
29	None			— / —	— / —	— / —	— / —	—	—	1st & 2nd[g]	0.216 / 0.085	475 / 1.05	0.56[f] / 0.22	12.7 / 5.0	20.3 / 8.0	-60	0	90	15	256 / 840	15.6 / 11.5	N.A.	N.A.	N.A.	N.A.	N.A.
30	Zy	35	1; 6; 1	0.126 / 0.259 (↑)	45.7/18.0; 82.6/32.5; 45.7/18.0	38.1/15.0; 62.2/24.5; 38.1/15.0	3.4 / 36.9 (↑)	371 / 0.82 (↑)	Unheld	1st & 2nd[g]	0.216 / 0.085	475 / 1.05	0.56[f] / 0.22	12.7 / 5.0	20.3 / 8.0	-69	-49	-10	15	258 / 847	15.8 / 11.7	30 / 99	15.62 / 11.52	5.38 / 3.97	10.24 / 7.55	81 / 29.2
31	Zy	35	3	0.047 / 0.097	82.6 / 32.5	62.2 / 24.5	1.5 / 16.6	166 / 0.37	G/P	2nd	0.216 / 0.085	187 / 0.41	0.79 / 0.31	7.6 / 3.0	10.2 / 4.0	-20	-27	-78	15	240 / 788	5.4 / 4.0	98 / 321	4.50 / 3.32	2.05 / 1.51	2.46 / 1.81	51.8 / 18.7
32	Zy	35	6	0.095 / 0.194	82.6 / 32.5	62.2 / 24.5	3.1 / 33.2	333 / 0.73	G/P	2nd & 3rd	0.274 / 0.108	482 / 1.06	0.56[f] / 0.22	12.7 / 5.0	20.3 / 8.0	-3	9	38	15	222 / 728	11.9 / 8.7	N.A.	N.A.	4.86 / 3.59	N.A.	N.A.
33	Zy	35	6	0.095 / 0.194	211 / 83.0	124 / 49.0	15.7 / 169	1700 / 3.75	G/P/W	1st & 2nd[g]	.22-.27 / .085-.11	481 / 1.06	0.56[f] / 0.22	12.7 / 5.0	20.3 / 8.0	50	-5	-4	15	256 / 840	15.8 / 11.6	117 / 385	12.46 / 9.19	1.58 / 1.17	10.88 / 8.02	115 / 41
34	Zy	35	6	0.095 / 0.194	82.6 / 32.5	62.2 / 24.5	3.1 / 33.2	333 / 0.73	G/P/W	1st & 2nd[g]	.22-.27 / .085-11	413 / 0.91	0.56[f] / 0.22	12.7 / 5.0	17.8 / 7.0	22	8	33	15	241 / 789	11.9 / 8.8	N.A.	N.A.	4.26 / 3.14	N.A.	N.A.
36	Zy	35	4; 6	0.158 / 0.324 (↑)	82.6/32.5; 211/83.0	62.2/24.5; 124/49.0	17.8 / 191 (↑)	1922 / 4.24 (↑)	G/P; G/P/W	2nd & 3rd[g]	0.234 / 0.092	419 / 0.92	0.69 / 0.27	10.2 / 4.0	17.8 / 7.0	4	-7	-34	15	265 / 870	14.7 / 10.9	0 / 0	14.75 / 10.88	4.23 / 3.12	10.52 / 7.76	>67 / >24

[a] Fabric barriers were located upstream of the insulation blanket, except for the last ply in Test CL-30, which was upstream of the interior wall panel (IWP).

[b] "K.E. absorbed by fuselage structure" was calculated from FAA JTCG model by NAWC-China Lake based upon their tests without fabric barriers; "K.E. absorbed by the fabric barrier" is the difference between the total K.E. lost and the K.E. absorbed by the fuselage structure (K.E. absorbed by insulation and I.W.P. are considered negligible).

[c] Specific Energy Absorbed — K.E. absorbed by the fabric barrier divided by its areal density; for tests where residual velocity was zero, the SEA of the barrier is a lower bound.

[d] "Zy" is Zylon, "Kev" is Kevlar, "Spec" is Spectra; mesh is in yarns per inch.

[e] G—glued (epoxied around periphery), P—pegged (holes cut in fabric fit around rubber protrusions on fuselage frame), W—washers (attached to protrusions to help retain fabric barrier).

[f] These impactors had small triangular fins extending outward on both faces.

[g] In these tests, the fragment impacted a stringer behind the fuselage skin.

Fragments as large as 5 in. wide by 8 in. long and weighing as much as 597 g (1.32 lb) were used for some tests (these are referred to as the "large" fragments), and these were launched at yaw angles as high as 45°. Other tests used 3-in.-wide by 4-in.-long fragments (referred to as "standard" fragments), weighing 166 to 181 g (0.37 to 0.40 lb), and were launched at 0° yaw. Fragment velocities ranged from 222 to 271 m/s (728 to 890 f/s) and kinetic energies from 4.5 to 18.1 kJ (3.3 to 13.4 kft-lb). In tests with the smaller impactors, the impactor passed through the skin only without impacting any of the stringers. In tests with the larger impactors, particularly tests involving large yaw, either the impactor encountered the stringers or the stringers were removed before testing to eliminate impact. Impact obliquities were either 0° or 15°.

The fabric barriers consisted of three to ten plies of Zylon 35 x 35 weave, except for one test which used Kevlar 32 x 32 weave and one with Spectra 32 x 32 weave. The arrangement of the fabric barriers within the fuselage wall is shown in figure 1. The fabric barriers were usually cut approximately the same width as the insulation blankets (see figure 1), and holes were cut near the vertical edges of the fabric at the same location as the holes in the insulation. For most tests, the fabric plies were glued to the insulation blanket (using epoxy along a thin rectangle near the fabric periphery) as shown in figure 2, and the holes in the fabric and insulation blanket were fastened around the protrusions in the fuselage frame ribs. Since the horizontal distance between the holes on the fabric was significantly greater than the distance between adjacent frame ribs (the fabric and insulation fold down into the recess between the ribs), there is substantial room for fabric stretching and deformation before the fabric tightens against the rib protrusions. For some tests, the barrier extended over three vertical fuselage frame segments but was glued to the insulation blanket only in the middle segment, the segment in which impact occurred.
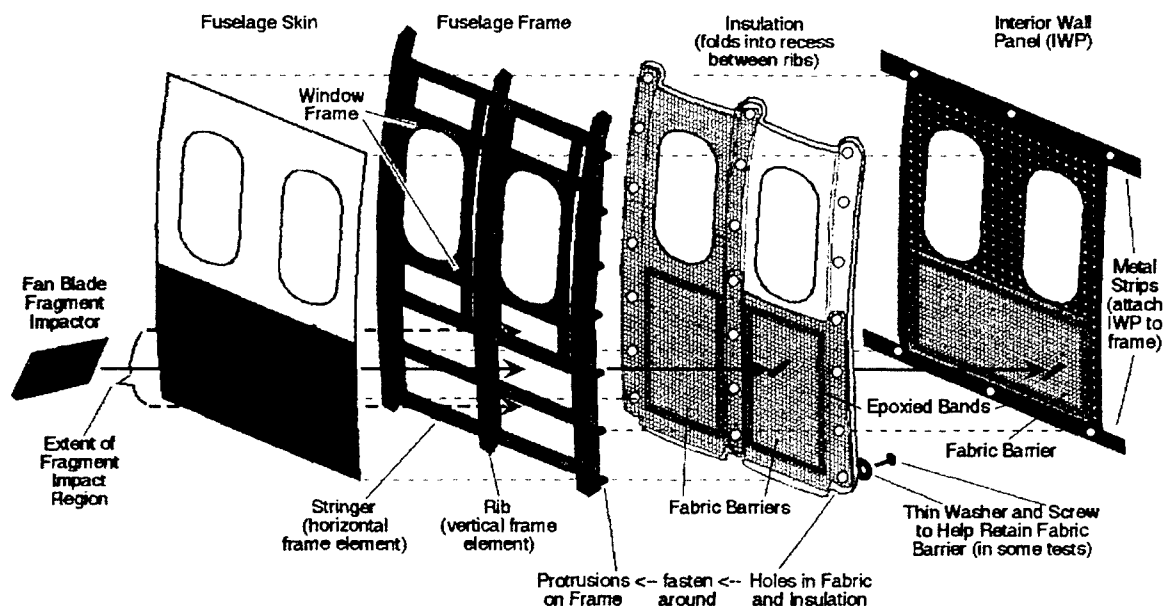
FIGURE 1. EXPLODED VIEW OF FUSELAGE WALL SHOWING REGIONS OF FRAGMENT IMPACT AND VARIOUS LOCATIONS OF FABRIC BARRIERS FOR OCTOBER 1999 TESTS AT CHINA LAKE

4

Holes in
Fabric and –> Fit Onto –> Protrusions on Frame Ribs
Insulation

≈1-in. wide
Band of Epoxy

20 in.

22 in.

Zylon Fabric

30 in.

Insulation Blanket

Fuselage Skin

20 in.

Stringer

(a) Zylon fabric barrier glued to insulation blanket

(b) Boeing 727 fuselage vertical frame segment
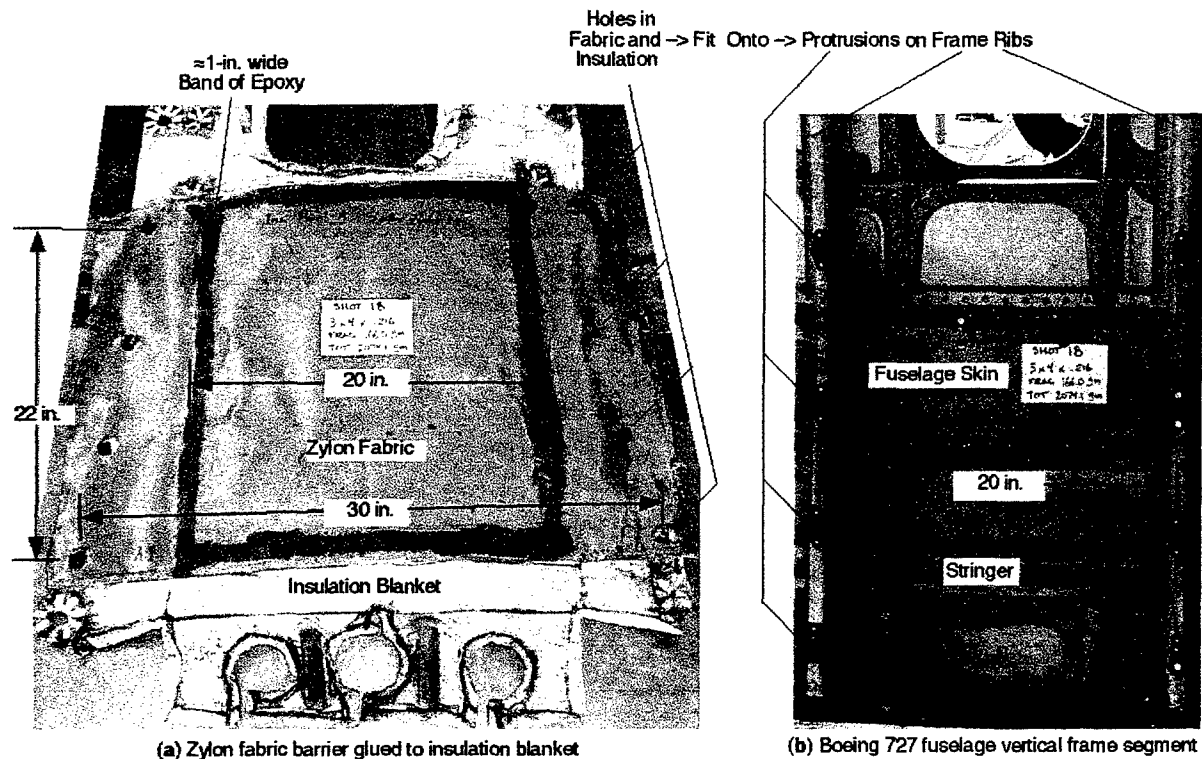
FIGURE 2. PRETEST PHOTOS OF ZYLON BARRIER AND REGION IN FUSELAGE
WHERE IT WAS PLACED

In most tests, the fabric extended vertically from the bottom of the window to the third stringer below the window, a distance of about 24 in. (62 cm). Although in a few tests, some of the fabric plies extended vertically up to one stringer past the window frame, a distance of 49 in. (124 cm). In one test, the last ply was glued to the interior wall panel, and in another test, the first ply was unheld (merely taped lightly in place).

After it had been determined that the flexible plastic clips, which are used to hold the insulation blanket in place on the frame protrusions, had failed to prevent the fabric barrier from slipping off the frame protrusions in some of the higher-energy tests. Thin, wide metal washers (called "fender" washers) were then screwed onto the frame protrusions (see figure 3) to assist in retention of the fabric. These washers were used only on the frame protrusions that were not in the same horizontal band as the impact region. For tests that extended over three vertical fuselage frame segments, the washers were used only on the outermost frame protrusions.

5
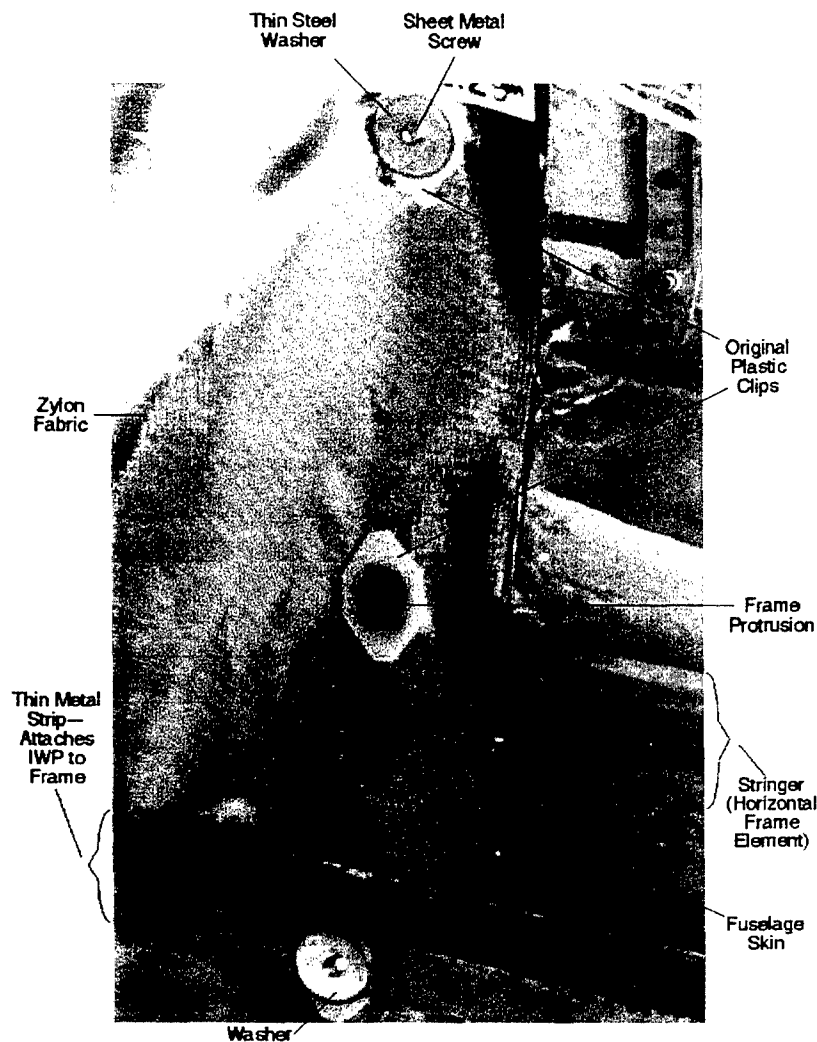
FIGURE 3. DETAIL OF FABRIC BARRIER INSTALLATION SHOWING ORIGINAL
PLASTIC CLIPS AND ADDED METAL WASHERS AND SCREWS

TEST RESULTS. Table 1 shows the quantitative test results, in terms of impactor orientations (determined from the last video camera image prior to impact), impact and residual velocities, kinetic energy losses, and specific energy absorbed (SEA), which is the kinetic energy absorbed by the barrier divided by its areal density. It should be noted that to determine the energy absorbed by the fabric barrier, the energy absorbed by the fuselage structure (calculated by NAWC-China Lake using their impact test data and the FAA Joint Technical Coordinating Group for Munitions Effectiveness (JTCG/ME) model* must be subtracted from the total kinetic energy lost by the fragment (determined from impact and residual velocities). Table 2 shows the qualitative test results and comments on barrier damage and corner retention. Figure 4 shows a graph of the energy absorbed by the fabric barrier versus barrier areal density for all of the tests.

---

* The calculations for energy absorbed by the fuselage structure were provided by Steve Lundin of NAWC-China Lake. These values have some uncertainties, particularly when structural elements other than the aircraft skin (e.g., stringers) are impacted, because the model does not take into account the geometry of these elements.

6

TABLE 2. FUSELAGE IMPACT TESTS—QUALITATIVE RESULTS AND COMMENTS

Test No. CL-	Fragment Penetrated Into Fuselage Interior	Number of Plies Perforated	Comments
18	Yes	3 of 3	—
19	No	0 of 3	Only a few yarns cut on each ply.
20	No	0 of 3	Nearly perforated all three plies.
21	No	0 of 3	Roughly half of the yarns necessary for perforation were cut on all three plies.
22	Yes	6 of 6	Barrier stretched over three vertical frame segments.
29	Yes	— — —	Baseline test without barrier, for large fragment test conditions.
30	Yes	1 of 8	Zylon barrier slipped off frame protrusions allowing fragment encased in fabric to enter fuselage. IWP broke away from the frame.
31	Yes	3 of 3	—
32	Yes	0 of 6	Barrier slipped off (or broke) frame protrusions allowing fragment encased in fabric to enter fuselage. IWP broke away from the frame.
33	Yes	6 of 6	Barrier stretched over three vertical frame segments, with washers on outermost frame rib protrusions only.
34	Yes	0 of 6	Three of four corners with washers failed to retain fabric, and part of IWP broke away from frame, allowing fragment to enter fuselage.
36	No	1 of 10	Barrier stretched over three vertical frame segments, with washers on outermost frame rib protrusions only.

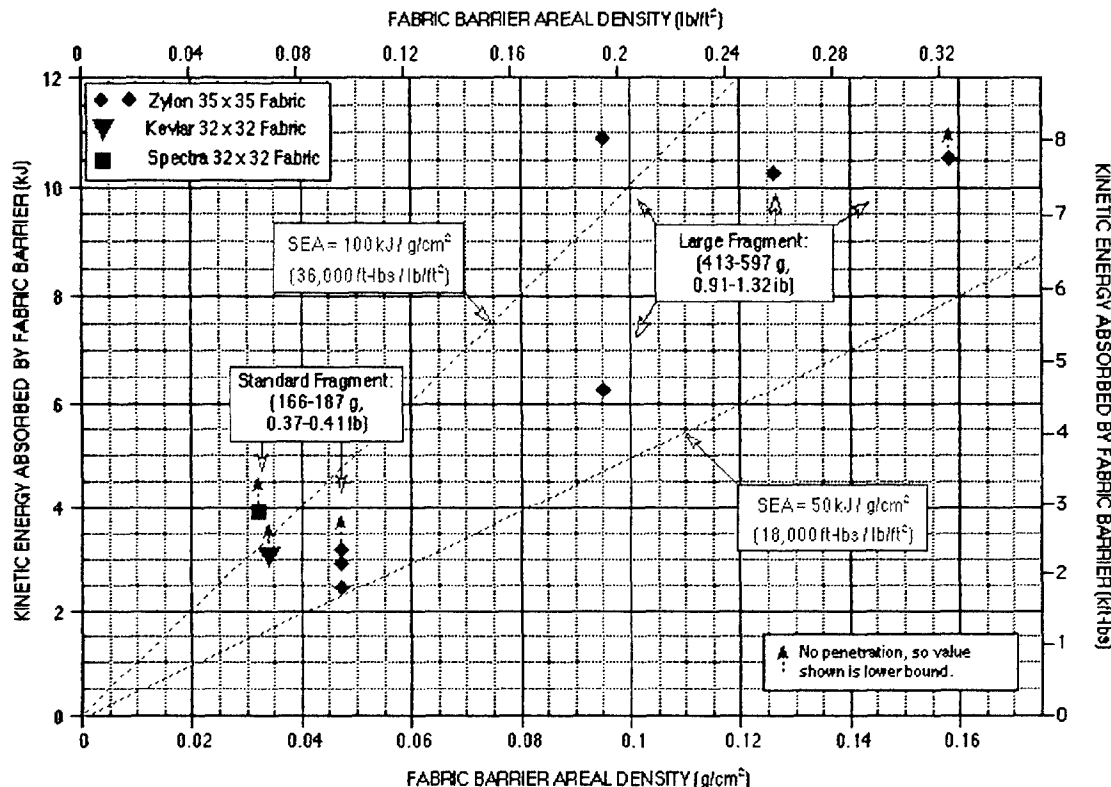The results of the tests showed that for large-real-turbine airfoil fragments, control of the impact orientation was difficult. The airfoils would rotate as they moved from the sabot to the fuselage structure. There was a noticeable decrease in accuracy when the larger 12-inch gas gun was used to fire larger fragments from the earlier full-scale testing with the 6-inch gun [4 and 5]. The motion and impact orientation are, however, well documented in the high-speed film providing valuable test data. The resulting database will be useful for evaluation of the final material and failure models. At the current program stage, the test point scatter makes relative comparison of the materials from this data difficult.

Standard Fragments. For the two tests involving the standard fragments impacting three-ply Zylon barriers, the SEA ranged from 52 to ≥ 66 kJ/g/cm^2 (19 to ≥ 24 kft-lb/lb/ft^2) when fragment penetration occurred. For the three tests in which the standard fragment was stopped by a three-ply barrier, the SEA ranged from ≥ 68 kJ/g/cm^2 (≥ 24 kft-lb/lb/ft^2) for Zylon, to ≥ 91 kJ/g/cm^2 (≥ 33 kft-lb/lb/ft^2) for Kevlar, to ≥ 122 kJ/g/cm^2 (≥ 44 kft-lb/lb/ft^2) for Spectra. Although these test results may appear to rank Spectra, Kevlar, and Zylon in decreasing order of ballistic efficiency as fragment barriers, examination of the recovered barriers (see comments in table 2) clearly show that Zylon was the least damaged of the three, with only a few yarns cut, followed by Spectra, with roughly half of the impacted yarns cut, and then Kevlar, with nearly all impacted

7

yarns cut. So, for example, Zylon's potential SEA was much greater than the lower bound value shown, while the potential SEA for Kevlar was only negligibly greater than the lower bound value. The Zylon barrier could have taken significantly more additional kinetic energy before it was penetrated than could the Kevlar barrier. Also, the impact orientations for these three tests were different. The different impact areas and number of yarns that needed to be cut for penetration complicates a direct comparison of the tests. A direct comparison of Zylon, Kevlar, and Spectra was described in an earlier report [4].

FIGURE 4. ENERGY ABSORPTION RESULTS OF FUSELAGE IMPACT TESTS

Large Fragments. For the five tests involving the large fragments impacting six- to ten-ply Zylon barriers, the results were as follows:

- In test 33, with the barrier extending across three vertical frame segments, the fragment penetrated the fuselage interior by perforating all the barrier plies. SEA was 115 kJ/g/cm^2 (41 kft-lb/b/ft^2).

- In tests 30, 32, and 34, with the barrier only one vertical frame segment wide, even though the fragment perforated, at most, the first ply of the barrier, the fragment penetrated into the fuselage interior because the barrier (along with all or part of the interior wall panel (IWP)) slipped off the frame due to retention failure at the frame protrusions (despite presence of washers in test 34). SEA was 81 kJ/g/cm^2 (29 kft-lb/lb/ft^2) for test 30, but was not determinable for tests 32 and 34 because the residual velocity of the fragment could not be measured.

8

- In test 36 where penetration was prevented, the barrier, which extended over three vertical fuselage frame segments, remained attached to the outermost frame ribs (the washers may have helped here) and perforated only the first of its ten plies. SEA was ≥ 67 kJ/g/cm^2 (≥ 24 kft-lb/lb/ft^2). It is very likely that fewer than ten plies would have prevented the penetration in this case.

CONCLUSIONS. These tests reconfirm that Zylon fabric is an exceptionally efficient fragment barrier. The SEAs in these tests are similar to those in the earlier series of fuselage impact tests. For fragments weighing around 175 g (0.4 lb), traveling at the maximum velocities expected for uncontained fragments around 265 m/s (780 f/s), three to four plies of Zylon, with areal densities around 0.05 g/cm^2 (0.1 lb/ft^2) extending across a single vertical frame element, will likely be sufficient to prevent penetration. Since these impact energy levels are generally below what is required to tear the IWP off the frame, thereby releasing the barrier corner restraints, the exact barrier attachment method does not appear to affect the ballistic results significantly. SEAs from these tests, where the corners of the fabric barriers were fastened around the frame protrusions while the barrier was glued near its periphery to the insulation blanket, were in the same range as those from the previous fuselage impact tests, where the barriers were glued but not fastened to the frame.

For large fragments weighing between 400 and 600 g (0.9 to 1.3 lb) and traveling at maximal expected uncontained fragment velocities, eight to ten plies of Zylon, with areal densities of around 0.15 g/cm^2 (0.3 lb/ft^2), appear to be sufficient to prevent penetration. This will be sufficient only if adequate measures are taken to prevent the corners of the barrier from slipping off their connection to the fuselage frame. The precise number of plies needed will be affected by the horizontal and vertical extent of the barrier. A barrier that is longer in the vertical direction, or extends over more than one vertical frame element, will require fewer plies. The impact energies involved in these tests are more than sufficient to

- tear the IWP from the frame
- rip the fabric from around the frame protrusions
- and in some cases, bend or fracture the attachment hardware

It is therefore important to design and test corner retention schemes that (1) avoid fabric corner failure, (2) retain the fabric on the frame, and (3) do not cause unacceptable levels of frame deformation or failure around the attachment hardware.

LARGE-SCALE IMPACT TESTS AT SRI'S REMOTE TEST SITE.

SRI recently completed the first series of 15 large-scale fragment impact tests using the 6-in.-bore gas gun located at Corral Hollow Experiment Site (CHES), SRI's remote test site near Tracy, California. This test facility enables large-scale fragments to be accelerated into full-scale fabric barriers at velocities in the range expected for uncontainment scenarios, and with negligible impactor rotation, thus allowing for the systematic variation of individual parameters that is necessary for optimizing the ballistic response of the barrier and for calibrating and verifying the computational models. The parameters to be varied during these tests included

9

barrier geometry (attachment method, lateral fabric size, degree of slack), number of plies, and the presence or absence of auxiliary structures (e.g., insulation and IWP).

As discussed the Computational Modeling of Fabric Barriers section, simulations with the detailed model indicated that holding the fabric at the four corners yielded higher energy absorption than gripping on two or four sides. Therefore, corner pegging was selected as the baseline barrier attachment method for these tests. In addition, implementation of the shell element design model allowed for the simulation of the complete fabric barriers for the large-scale tests.

TEST CONFIGURATION AND PROCEDURES. The 6-in.-bore gas gun test facility is shown in figure 5, and a matrix of test parameters is given in table 3. For this first series of tests, the intended impact obliquity was 0° (the target barrier was perpendicular to the axis of impact), and the intended roll, yaw, and pitch angles were 45° (from vertical—the fabric was positioned so that the yarns were vertical and horizontal), 0°, and 0°, respectively.

Sections of a commercial transport aircraft fuselage—the same type of plane used in the China Lake fuselage impact tests—were obtained for use in some of these tests, along with the insulation blankets and IWPs.* A rigid fixture (made of Unistrut** beams reinforced by box beams) was constructed near the muzzle of the gun for mounting the fuselage section (see figures 5(c) and 6).

The fabric barrier was typically glued to the outboard side of the insulation blanket and holes were cut in the fabric at the same locations as the holes in the insulation (as shown in figure 2 for the China Lake tests). The fabric was then pegged to the frame by slipping the holes at the four corners only around the frame protrusions (see figure 7), using thin bolts and washers to secure the IWP to the frame through these protrusions. With the fabric and insulation positioned on the frame ribs, there is a horizontal slack in the fabric of ~5.5 in. at the upper two holes, a horizontal slack of ~10 in. at the lower two holes, and negligible vertical slack. This is referred to as the "standard" barrier geometry.

In tests 102 and 104, the fabric was glued only and not pegged. In tests 106 through 109, the fabric was pegged only and no insulation blanket or IWP was used. The fuselage skin was removed in the region of impact to avoid having to replace it for each test, and because the energy absorbed by the skin was well characterized by tests performed by NAWC at China Lake, it would not vary for the same fragment orientation.

---

* Although the insulation blankets obtained were identical to those in the China Lake tests, the IWPs were not. They were the old-style, ~0.025-in.-thick aluminum panels, stretching over one vertical frame segment, instead of the more modern, ~0.25-in.-thick, plastic honeycomb/fiber-reinforced resin composites, stretching over two frame segments. They proved not to be as effective an auxiliary component of a fragment barrier, because upon perforation, the aluminum peeled back, opening up a large hole, which did not offer nearly as much drag to the unperforated fabric barrier as did the small perforation holes created in the composite IWPs.

** Manufactured by Unistrut Corporation, division of Tyco International Ltd., Itasca, Illinois.
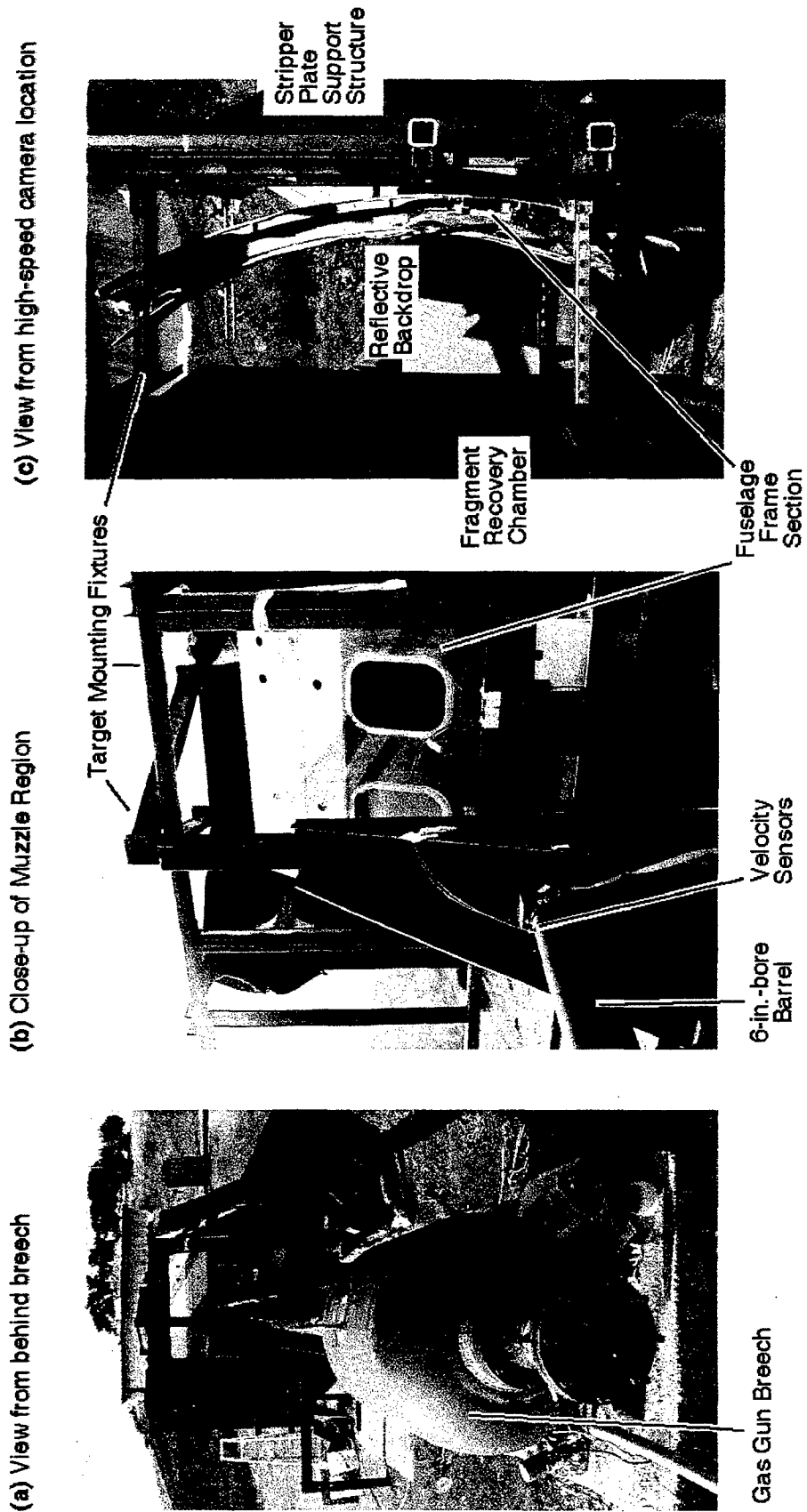
(a) View from behind breech

(b) Close-up of Muzzle Region

(c) View from high-speed camera location

FIGURE 5. LARGE-SCALE FRAGMENT IMPACT TEST SETUP AT SRI'S REMOTE TEST SITE

11

TABLE 3. TEST MATRIX FOR FIRST SERIES OF LARGE-SCALE IMPACT TESTS AT SRI'S REMOTE TEST SITE

Test No.	Impactor[a] Mass (g) / (lb)	Velocity (m/s) / (f/s)	Kinetic Energy (kJ) / (kft-lb)	Material, Mesh, Number of Piles	Areal Density (g/cm²) / (lb/ft²)	Dimensions Horiz. (cm) / (in.)	Vert. (cm) / (in.)	Auxiliary Structures	Attachment Method(s)[c] / Corner Hole Pattern (center-to-center, vert. x horiz.) and Slack Geometry[d]	Results — Fragment Stopped? If so, max. axial fabric deflection / Corner Failure?[e]	Residual Velocity (m/s) / (f/s)	K.E. Absorbed (kJ) / (kft-lb)	SEA[b] (kJ/(g/cm²)) / (kft-lb/(lb/ft²))
101[f]	172 / 0.39	231 / 758	4.59 / 3.38	Zylon 35 / 3	0.047 / 0.096	83.8 / 33.0	62.2 / 24.5	Fuselage Ins./IWP	Glued and Pegged / Standard	No / None	202 / 663	1.08 / 0.80	23.0 / 8.3
102	175 / 0.40	231 / 758	4.67 / 3.44	Zylon 35 / 3	0.047 / 0.096	83.8 / 33.0	62.2 / 24.5	Fuselage Ins./IWP	Glued / Standard Slack	No / ——	188 / 617	1.58 / 1.16	33.5 / 12.1
103	175 / 0.40	231 / 758	4.67 / 3.44	Zylon 35 / 6	0.094 / 0.193	83.8 / 33.0	62.2 / 24.5	Fuselage Ins./IWP	Glued and Pegged / Standard	No / 1	163 / 535	2.34 / 1.73	24.9 / 9.0
104	175 / 0.40	228 / 748	4.55 / 3.36	Zylon 35 / 6	0.094 / 0.193	83.8 / 33.0	62.2 / 24.5	Fuselage Ins./IWP	Glued / Standard Slack	No / ——	138 / 453	2.88 / 2.12	30.6 / 11.0
105	175 / 0.40	191 / 626	3.19 / 2.35	Zylon 35 / 6	0.094 / 0.193	83.8 / 33.0	62.2 / 24.5	Fuselage Ins./IWP	Glued and Pegged / Standard	Yes, <43 cm (<17 in.) / None	0 / 0	> 3.19 / > 2.35	> 34.0 / > 12.2
106	175 / 0.40	191 / 626	3.19 / 2.35	Zylon 35 / 4	0.063 / 0.129	83.8 / 33.0	62.2 / 24.5	Fuselage	Pegged / Standard	No[g] / All	< 60 / < 197	> 2.88 / > 2.12	> 45.7 / > 16.4
107	175 / 0.40	208 / 682	3.79 / 2.79	Zylon 35 / 4	0.063 / 0.129	83.8 / 33.0	62.2 / 24.5	Fuselage	Pegged / Standard except top holes lowered 2 in.	No / 1	132 / 433	2.26 / 1.67	35.9 / 12.9
108	175 / 0.40	124 / 407	1.35 / 0.99	Zylon 35 / 2	0.031 / 0.063	83.8 / 33.0	62.2 / 24.5	Fuselage	Pegged / Standard except top holes lowered 2 in.	Yes, -56 cm (-22 in.) / 2 or 3	0 / 0	> 1.35 / > 0.99	> 43.4 / > 15.6
109	175 / 0.40	144 / 472	1.81 / 1.34	Zylon 35 / 2	0.031 / 0.063	83.8 / 33.0	62.2 / 24.5	Fuselage	Pegged / Standard except top holes lowered 2 in.	No / 2 or 3	46 / 150	1.63 / 1.20	52.7 / 19.0
110	175 / 0.40	146 / 479	1.87 / 1.38	Zylon 35 / 2	0.031 / 0.063	86.4 / 34.0	62.2 / 24.5	—	Pegged / 20 in. sq. hole pattern, std. slack	Yes, -51 cm (-20 in.) / 2 or 3	0 / 0	> 1.87 / > 1.38	> 60.2 / > 21.7
111	175 / 0.40	149 / 489	1.94 / 1.43	Zylon 35 / 2	0.031 / 0.063	86.4 / 34.0	62.2 / 24.5	—	Pegged, w/holes doubled[h] / 20 in. sq. hole pattern, no slack	No / None[i]	72 / 235	1.50 / 1.10	48.2 / 17.4
112	175 / 0.40	136 / 446	1.62 / 1.19	Zylon 35 / 2	0.031 / 0.063	86.4 / 34.0	62.2 / 24.5	—	Pegged, w/holes quadrupled[h] / 14.5 x 20 in. hole pattern, 5 in. horiz. slack	No / None[i]	46 / 150	1.43 / 1.06	46.3 / 16.7
113	175 / 0.40	135 / 443	1.59 / 1.18	Zylon 35 / 2	0.031 / 0.063	86.4 / 34.0	62.2 / 24.5	—	Pegged, w/holes quadrupled[h] / 14.5 x 20 in. hole pattern, 5 in. horiz. slack	No[g] / All	< 22 / < 72	> 1.55 / > 1.15	> 50.1 / > 18.0
114	177 / 0.41	137 / 449	1.66 / 1.23	Zylon 35 / 2	0.031 / 0.063	71.1 / 28.0	126 / 49.5	—	Pegged / 41.5 x 20 in. hole pattern, no slack	No / None	83 / 272	1.05 / 0.78	34.0 / 12.2
115	177 / 0.41	121 / 395	1.29 / 0.95	Zylon 35 / 2	0.031 / 0.063	71.1 / 28.0	126 / 49.5	—	Pegged / 41.5 x 20 in. hole pattern, no slack	Yes, -51 cm (-20 in.) / 1	0 / 0	> 1.29 / > 0.95	> 41.5 / > 14.9

[a] All tests had 0° ± 1° impact obliquity, 0° ± 1° pitch, 0° ± 10° yaw, and 45° ± 15° (usually ± 4°) roll.

[b] Specific Energy Absorbed (SEA) — K.E. absorbed divided by areal density; for tests where residual velocity was zero, the SEA is a lower bound.

[c] Glued — as in Figure 2; Pegged — at 4 corners through 1-in.-diam. holes; w/holes doubled — vertical seams on 2 sides; w/holes quadrupled — seams on 4 sides.

[d] Standard geometry (see Figure 2, but pegged at 4 corners only), includes varying horizontal slack (5.5 in. at top —10 in. at bottom) and negligible vertical slack.

[e] Fabric corner detaching from frame, by fabric tearing from hole to edge, by hole in fabric growing and slipping over retention hardware, or by hardware failure.

[f] Fiber optic velocity sensors did not work, so impact velocity was obtained from high-speed camera record.

[g] Fragment did not perforate the fabric but remained enshrouded in it. Residual velocity shown is last clearly visible data point, but deceleration likely continued.

[h] Test 111 had 4 in. of fabric between doubled holes; Test 112 had 1.5 in. between quadrupled holes; Test 113 had 0.75 in. between quadrupled holes.

[i] No corners failed, but the fabric ligaments between the multiple holes failed (Test 111) or had significant damage (Test 112).
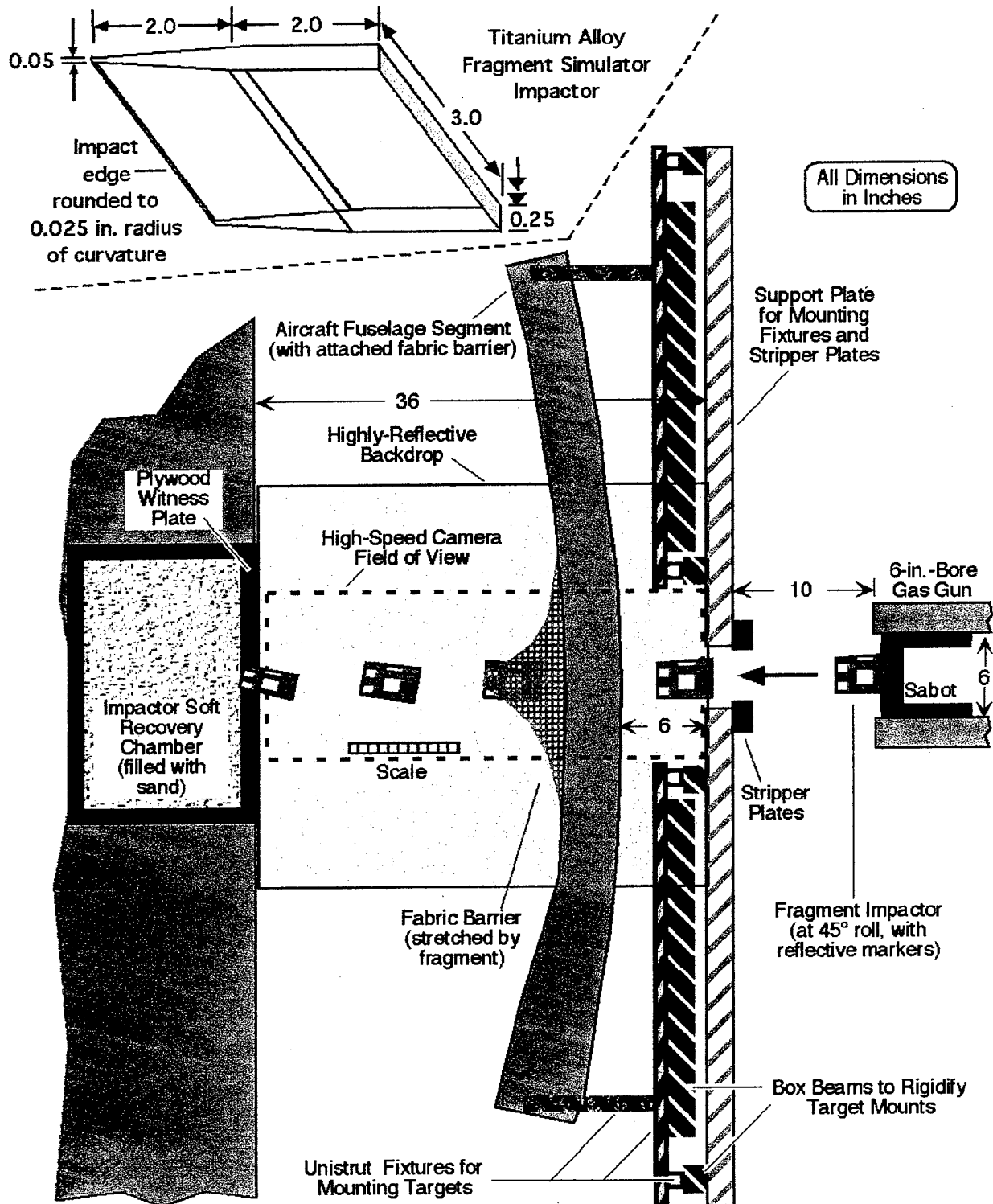
All Dimensions in Inches

FIGURE 6. SCHEMATIC OF IMPACT TEST CONFIGURATION WITH FABRIC BARRIER ATTACHED TO FUSELAGE SEGMENT
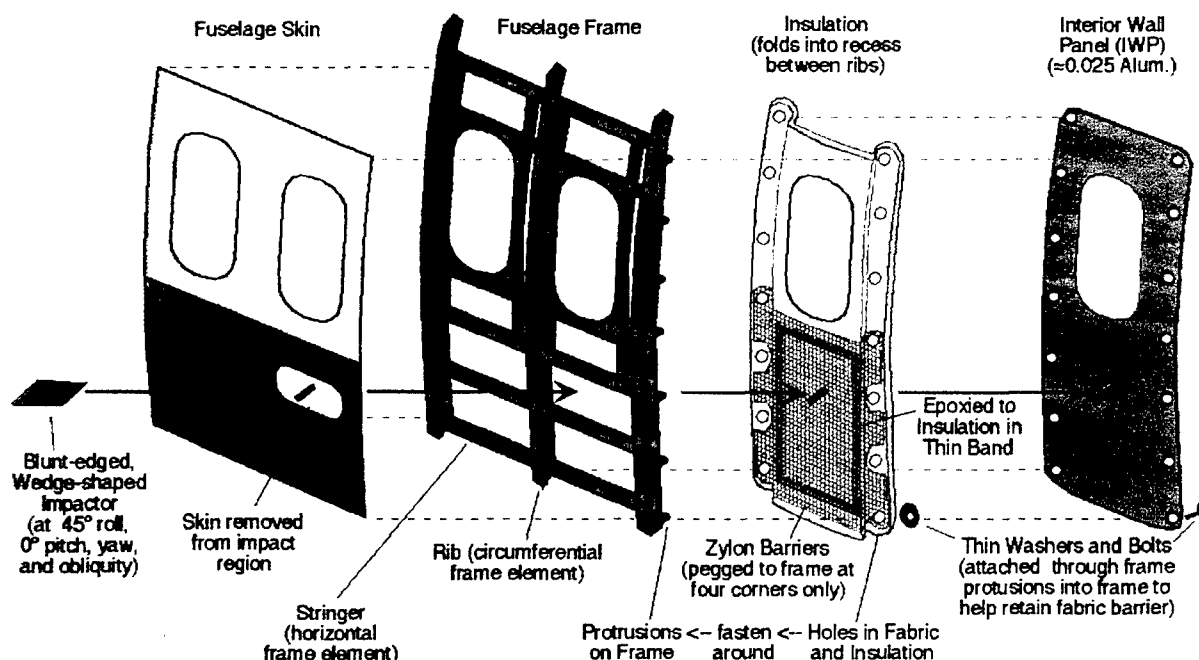
FIGURE 7. BARRIER MOUNTING SCHEME FOR TESTS USING FUSELAGE SECTION WITH FABRIC PEGGED AT FOUR CORNERS

During some of the tests using the fuselage section, the thin bolts securing the corners of the fabric to the frame failed, allowing the corner to come free. When larger bolts were substituted, the region of the frame where the bolt was attached deformed or failed, with a similar result. Also, the thin aluminum IWP sometimes deformed and became loose at one or more of its corners. Tests 110 through 115 were performed without a fuselage frame to reduce the likelihood of attachment failure (an undesired variation in the barrier boundary conditions) and to make the boundary conditions simpler and easier to model. Instead, the fabric was fastened at its four corners to the Unistrut mounting frame (as shown in figure 8) using stronger hardware, which was later redesigned to decrease the likelihood of the fabric slipping off the hardware, even after significant deformation of the fabric corner. The new hardware reduced the incidence of corner failure by slip-off or hardware failure, but there were still occasional incidences of corner failure by fabric tearing if the hole was too close to the fabric edge.

The titanium alloy fragment impactors used in these tests (see figure 6) are similar to the standard fragments described above for the China Lake tests. They are 4.0 in. (10.2 cm) long by 3.0 in. (7.6 cm) wide, with a thickness of 0.25 in. (0.62 cm) that tapers from the mid-point down to 0.05 in. (0.13 cm) at the impact end, where the edges are slightly rounded. The impactors weigh roughly 0.4 lb (175 g), and they are mounted at the front of a sabot, which is accelerated down the barrel of the gas gun. Two fiber-optic light sensors located near the end of the barrel record the passage of alternate light and dark circumferential strips on the outside of the sabot, allowing the velocity of the sabot to be determined. The sabot is stopped by the stripper plates, while the fragment travels a short distance on its own before impacting the target.
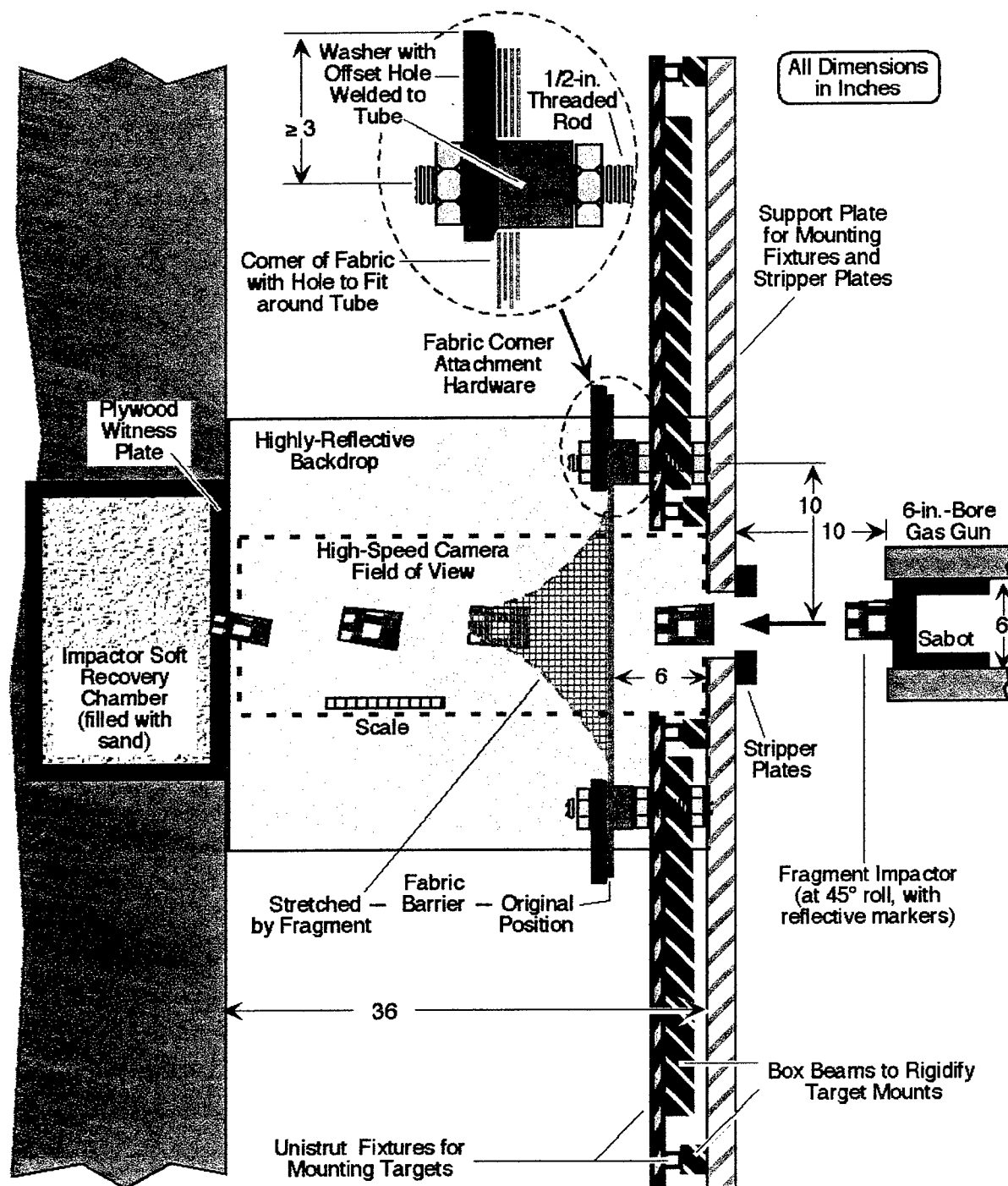
FIGURE 8. IMPACT TEST CONFIGURATION WITH FABRIC BARRIER FASTENED AT FOUR CORNERS AND DETAIL OF CORNER ATTACHMENT HARDWARE

A high-speed camera (at approximately 20,000 frames per second) records the motion of the fragment before impact, the deformation of the fabric barrier around the fragment, and the motion of the fragment during and after perforation of the barrier, in the case of penetration. A highly reflective backdrop enables observation of silhouettes of the fragment and of the proximal edge of

15

the deforming fabric barrier. Highly reflective tape pieces placed on the faces and sides of the fragment allow for easier determination of the orientation during and after penetration. After penetration, the fragment impacts a plywood witness plate, where it bounces off, becomes lodged, or penetrates through to the sand-filled soft recovery chamber.

TEST RESULTS—FRAGMENT AND BARRIER MOTION. The results for the first series of large-scale impact tests are shown in table 3, including both qualitative results (whether the fragment was stopped, whether it perforated the fabric, and whether the corners of the fabric came loose from the mounting frame) and quantitative results (the residual velocity of the fragment, the kinetic energy absorbed by the fabric barrier, and the SEA).

Examination of the films from the high-speed camera showed negligible deviation of the fragment from the intended pitch and yaw angles to within the limits of the angular resolution* ($\pm 1°$ for pitch, $\pm 10°$ for yaw). The deviation of the roll angle was generally less than $\pm 4°$, never greater than $\pm 15°$, and most likely due to rotation of the sabot within the barrel.

Relevant frames from the film were digitized to obtain the velocity and orientation history of the fragment and the deformation history of the fabric barrier. This data is put into graphical form and made available for comparison with the computational simulations. Test 114, which resulted in fragment penetration, and test 115, in which the fragment was stopped, have been selected as examples. The graphs plotted from the digitized film data from these tests are presented and discussed in the next few paragraphs.

Figure 9 shows outlines of the fragment and the edge of the fabric at various times before impact, during, and after penetration in test 114. Every frame before impact is shown and approximately every fifth frame after impact. The fragment edges have dashed lines when the fragment shape is discernible, but the fragment is cloaked by the fabric. The fragment edges have solid lines when the fragment is not cloaked, both before impact and when the fragment emerges after perforation of the barrier. The highly reflective tape at the fragment corners allows for a clear distinction between cloaked and uncloaked fragments. In test 114, the front corners of the fragment perforated the fabric relatively early in the fabric deformation (by frame 14 for the lower corner and by frame 22 for the upper corner). However, the front edge of the fragment did not completely break free until after frame 37, and the lower fragment edge (hence the entire fragment) did not break free until just before frame 52. The rotation of the fragment during and after penetration is clearly visible.

Figures 10 and 11 show the axial position and the axial velocity histories of the fragment corners for test 114, respectively. Although the position histories are very smooth, the velocity histories are somewhat noisy. The digitized films can be read only to the nearest pixel, and a one-pixel change in the reading produces a 13-m/s change in the velocity. Nevertheless, the residual velocity can be obtained by averaging the values of the axial velocity for the four corners once

---

* One pixel on the digitized film was equivalent to 0.05 in. (0.13 cm) at the fragment location. The angular resolution was based upon ± 1 pixel and the appropriate trigonometric function (angular resolution of the roll at 45° was $\pm 1.5°$).

fragment is free of all interaction with the fabric (due to rotation, the values for the four corners differ from each other and vary over time).
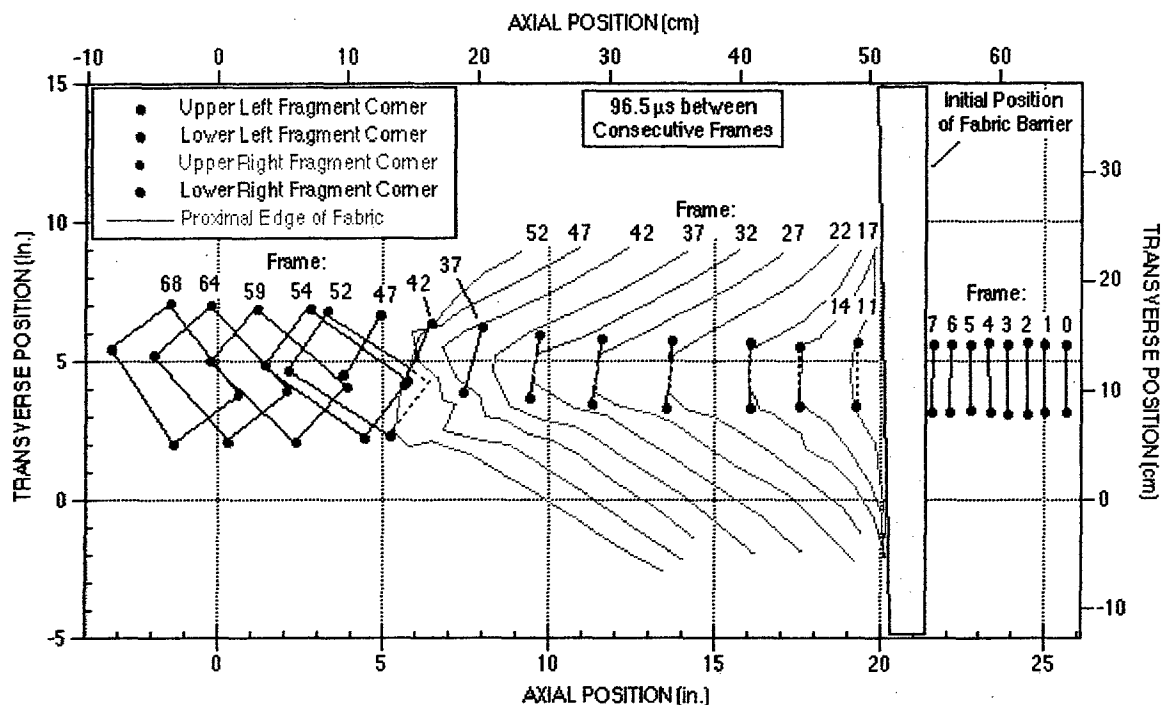

FIGURE 9. SILHOUETTES OF FRAGMENT AND FABRIC MOTION
DURING IMPACT TEST 114
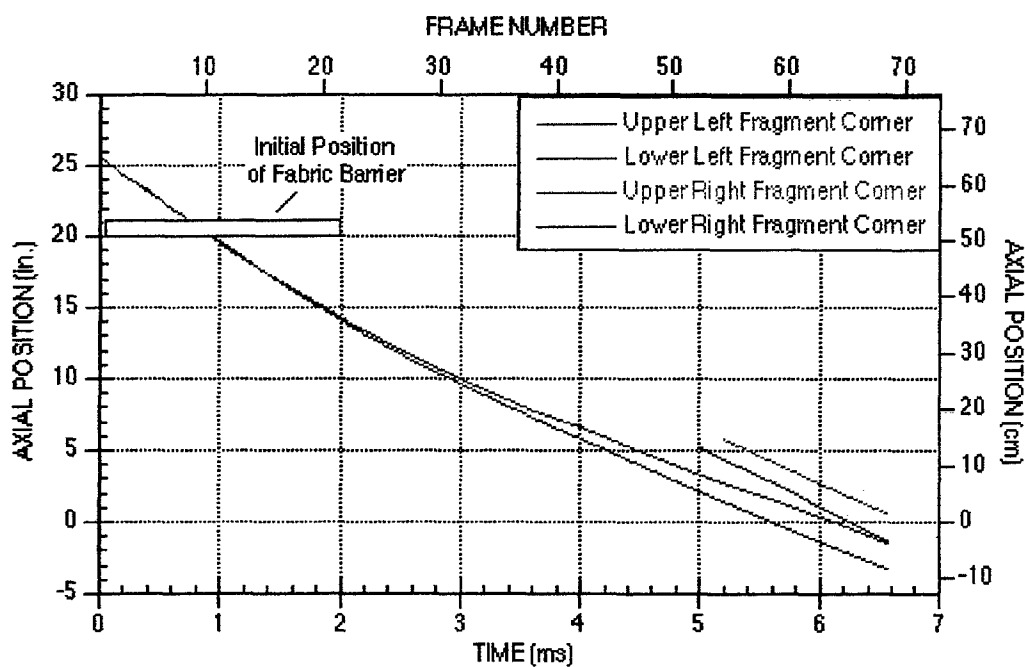
FIGURE 10. AXIAL POSITION OF VISIBLE FRAGMENT CORNERS IN TEST 114

17

FRAME NUMBER
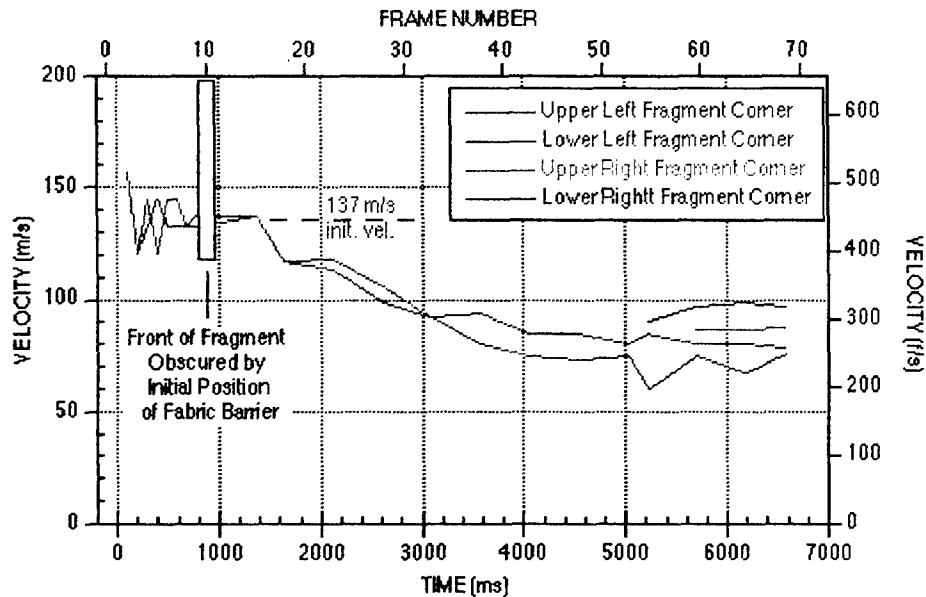
FIGURE 11. AXIAL VELOCITY OF VISIBLE FRAGMENT CORNERS IN TEST 114

Figures 12 through 14 are the same three graphs for test 115. For this test, only the lower front corner of the fragment perforated the fabric (by frame 28). The fragment continued to deform the fabric, while it decelerated and rotated. The location of the lower back fragment corner is apparent in frame 68, but after that no clear outline of the fragment is visible. The fragment did not yet reach zero axial velocity at that time. Since the fragment did not completely perforate the fabric, and since there was no mark on the witness plate to denote any impact, the residual fragment velocity was deemed to be zero (three of the four fabric corners remained fastened to the frame).

FIGURE 12. SILHOUETTES OF FRAGMENT AND FABRIC MOTION DURING
IMPACT TEST 115

18

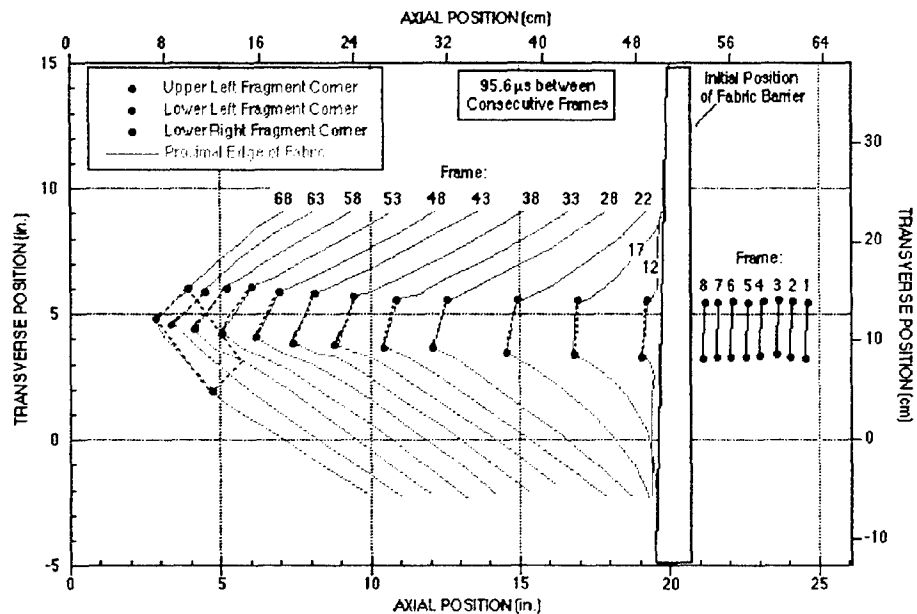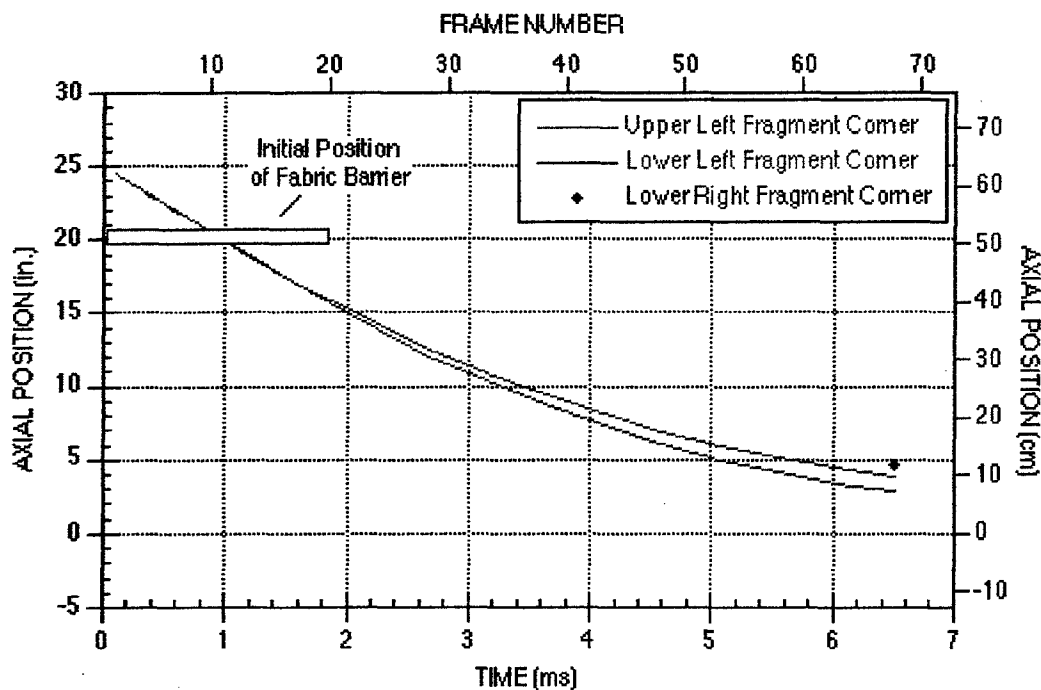FIGURE 13. AXIAL POSITION OF VISIBLE FRAGMENT CORNERS IN TEST 115
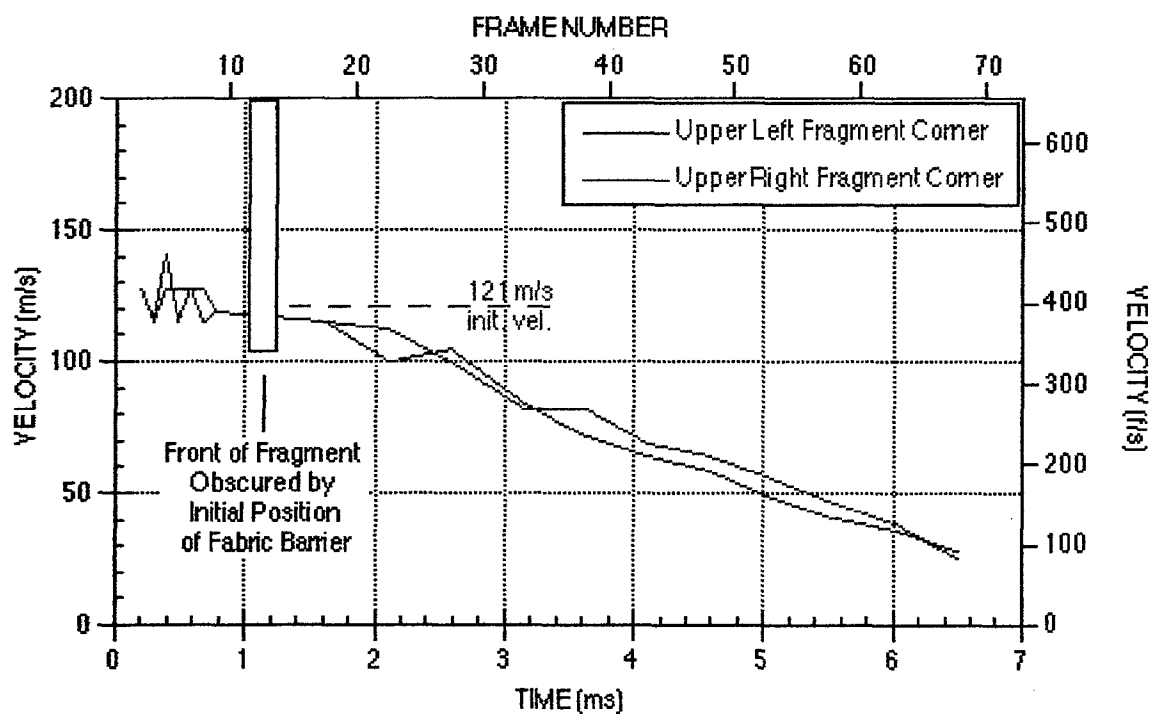

FIGURE 14. AXIAL VELOCITY OF VISIBLE FRAGMENT CORNERS IN TEST 115

19

TEST RESULTS—ENERGY ABSORPTION. The energy absorption and areal density values shown in table 3 are plotted in figure 15. The SEAs range from 23 to >60 kJ/g/cm^2 (8 to >20 kft-lb/lb/ft^2), which are somewhat less than the 52 to $\geq$66 kJ/g/cm^2 (19 to $\geq$24 kft-lb/lb/ft^2) range of SEAs for the same type of fragment impacting the same Zylon fabric in the second series of fuselage impact tests at China Lake. This is reasonable, since the impact areas (and hence the number of yarns that need to be cut to allow penetration) in these tests were significantly less (because of the nearly 0° yaw attained) than in the China Lake tests (where the yaws were large).
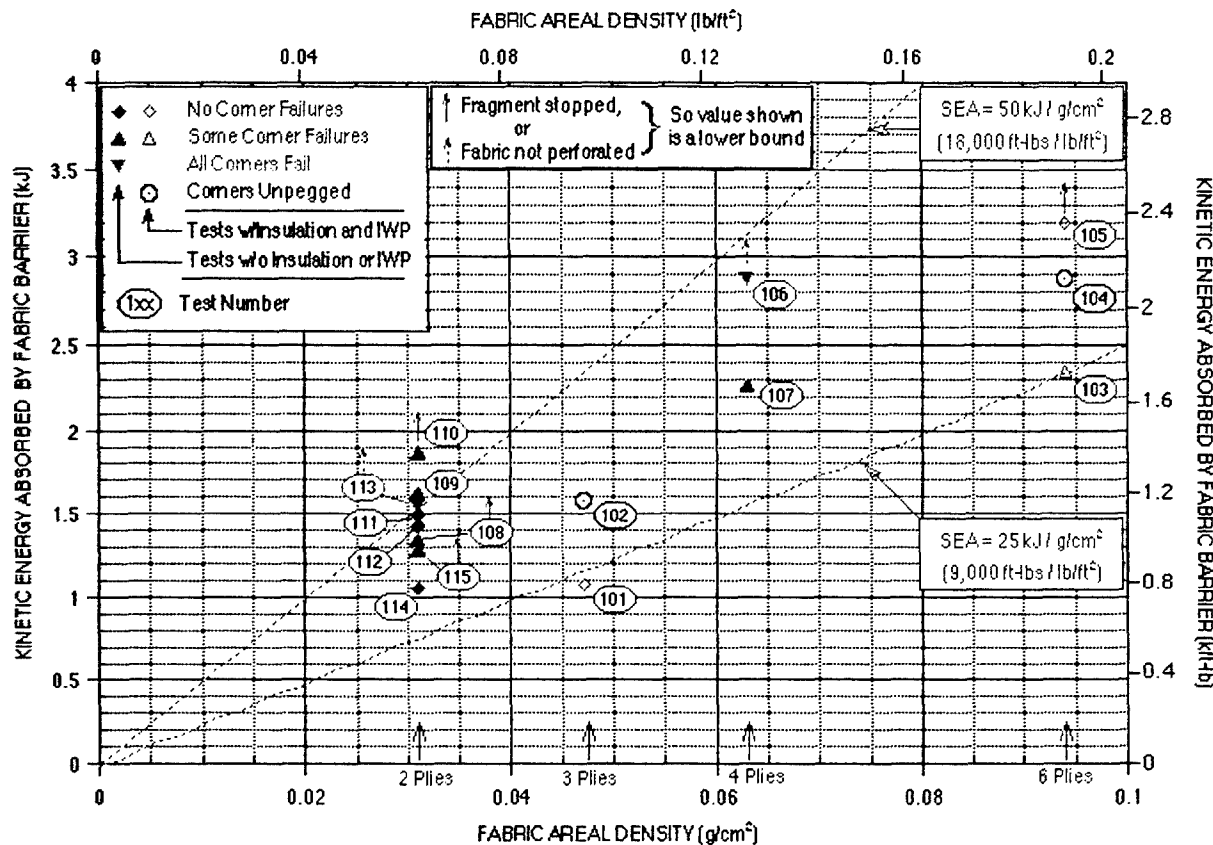
FIGURE 15. RESULTS OF LARGE-SCALE FRAGMENT BARRIER IMPACT
TESTS WITH ZYLON FABRIC

The following paragraphs discuss the conclusions that can be drawn thus far concerning the effect of the fabric barrier design parameters that have been varied in these tests.

Auxiliary Materials. The presence of the insulation and IWP did not improve the effectiveness of pegged barriers: SEAs for tests with insulation and IWP (tests 101, 103, and 105) were less than for those without insulation and IWP (tests 106 through 115). For unpegged (glued only) barriers (tests 102 and 104), the SEAs were significantly lower than in an earlier test series (March 1999) at China Lake. This likely relates to the ineffectiveness of the aluminum IWPs to produce any drag resistance, as compared to the composite honeycomb IWPs used in the earlier tests.

Number of Plies. The energy absorbed is nearly proportional to the number of plies (at least for tests with three and six plies, resulting in penetration). SEAs for tests 101 and 103, with three plies of Zylon, are nearly the same as those for tests 102 and 104, with six Zylon plies (all other parameters for each pair of tests are the same). Since only a few tests were conducted with more than four plies, a more definitive relationship between energy absorbed and number of plies cannot be made until further tests are performed later this year.

Slack. The presence or absence of slack did not affect the barrier efficiency significantly. Tests 111 and 112 were fairly similar, except that test 111 had no slack and test 112 had 5 in. of horizontal slack, the resulting SEAs were very close. It is likely that the only effect slack has is to allow for more deflection of the fabric before the fabric becomes taut (during which time fragment deceleration is relatively low, due only to the inertia of the fabric), at which time the fabric applies a larger decelerating force to the fragment. It may be necessary to reduce fabric barrier slack in cases where the allowable fabric deflection distance is limited.

Lateral Fabric Dimensions. Previous testing at China Lake indicated that fabric barriers with larger lateral dimensions would absorb more energy. However, increasing the length of the fabric in one direction while keeping the other direction constant, as was done in tests 114 and 115, did not have that expected result. However, the results were not conclusive since similar tests with the baseline fabric dimensions that were needed for direct comparisons did not sustain the same fabric corner hole failure results. Additional tests in the next program year will further examine the effect of length increases in one and two directions.

Corner Failure. Corner failure (the detaching of the corner from the fuselage or other mounting frame) played an important role in the energy absorption of pegged barriers. In a couple of the tests, corner failure occurred by failure of the retention bolts or the fuselage region to which these bolts were attached. Usually, corner failure occurred when the fabric around the holes deformed sufficiently to allow the hole to slip over the retention hardware (bolts and washers) or when the fabric tore between the hole and an edge.

The SEAs were greatest for tests

- in which all the corners failed (tests 106 and 113) or most of the corners failed (tests 108 through 110)

- where the holes were doubled or quadrupled

- where there was failure of the fabric around one of the holes (test 111) or significant damage between the holes in each corner (test 112)

The energy-absorbing mechanisms include fabric distortion, yarn stretching, yarn tensile failure, and yarn pullout (as shown in figure 16, for cases of significant fabric damage around holes but where the corners did not fail).

21

(a) Test 115

1 in. (equals diameter of fabric holes)
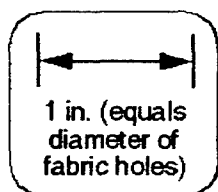
Towards Impact Region

Initial Size and Location of Hole
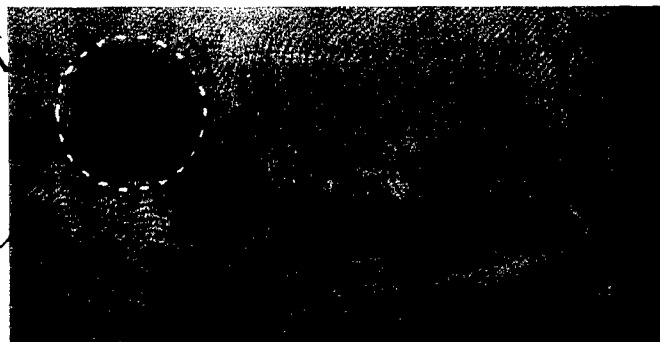
(b) Test 111

Closest Hole to Impact Region of a Doubled Pair

Second Hole of Pair (4 in. below Hole Shown) Exhibited Only Moderate Enlargement and No Tearing Towards Edge

(c) Test 112

Quadrupled Group of Holes
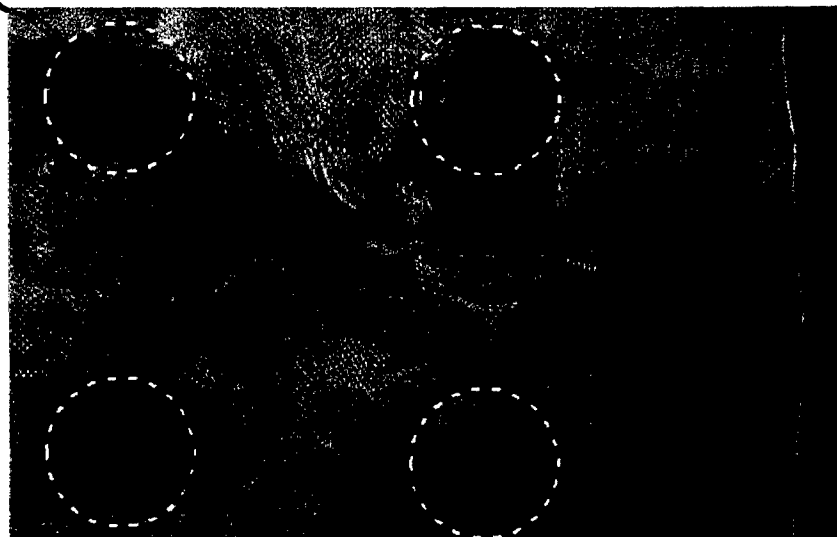
FIGURE 16. FABRIC DEFORMATION AND FAILURE AROUND PEGGED HOLES NEAR FABRIC BARRIER CORNERS THAT DID NOT COMPLETELY FAIL

22

DISCUSSION OF CONCLUSIONS. The fact that corner failure was shown to contribute heavily to fabric barrier energy absorption does not mean that barriers should be designed so that the corners fail. Obviously, if all of the corners fail, the fragment cannot be stopped, unless the drag through a small hole in an IWP or other auxiliary structure is sufficient to stop the fragment-encasing fiber barrier (as was the case in the earlier China Lake series with unpegged barriers). If some (or even one) of the corners fail, the maximum axial deflection of the barrier, before the fragment is stopped, increases (compare, in table 3, results for test 105 with those of tests 108 and 110) and may exceed the safety limits for the particular application. Corner failure reduces the total energy absorption possible; once the corner fails, further absorption of energy due to fabric deformation and failure in that region cannot occur.

What this means is that fabric barriers should be designed to take advantage of the energy absorption potential of material failure around corner holes, while at the same time preventing total corner failure. By weakening the fabric (through the cutting of holes, for example) and encouraging material failure away from the impacted regions, the fabric is less likely to fail in the impacted regions and, therefore, more able to resist fragment penetration. In addition, the maximum force on the retention hardware is reduced by weakening the material near the corner. This reduces the likelihood of hardware or frame failure.

The SRI fabric computational models must be able to simulate accurately the behavior of fabric around holes. It is important, therefore, to understand the deformation and failure mechanisms of the fabric around a hole and between holes and edges or corners. How does the fabric tear between two neighboring holes? How far does a hole have to be from an edge to prevent tear-through? How does the size and shape of the hole or the retention peg in the hole affect the deformation and failure of fabric in the vicinity? Computational simulations need to be run to examine these problems, and experiments need to be performed to provide the data necessary for model refinement and verification.

A laboratory test, called the fabric corner failure test, was designed to examine fabric behavior in the vicinity of a held corner. Figure 17 shows the design for a fabric that is pegged through a hole near the corner. Using many of the same fixtures from the previously reported [4] quasi-static penetration (pull) and yarn pullout tests, this test will produce detailed video images and acoustic records of fabric deformation and failure around a pegged hole, while recording the deflection of the peg and the load on the fabric. The size and shape of the hole and the peg and the proximity to the fabric edge can be varied. Other potentially energy-absorbing variations can be tested, such as multiple-pegged holes or additional unpegged holes in the vicinity of the pegged holes. Holding the fabric corner by means other than pegging through a hole (such as winding the fabric around a flattened rod) should also be tested. A test series, with the parameters to be determined in conjunction with computational simulations, is planned for the next program year.

23

FRONT VIEW · **SIDE VIEW**

- Crosshead of Mechanical Testing Machine
- Load Cell
- Clevis Fixture
- Rod through Clevis and Acrylic Plates
- Videocamera Field of View
- Clear Acrylic Plates
- Rod through Fabric and Acrylic Plates
- To Video-Camera
- Woven Fabric
- Clamping Bar
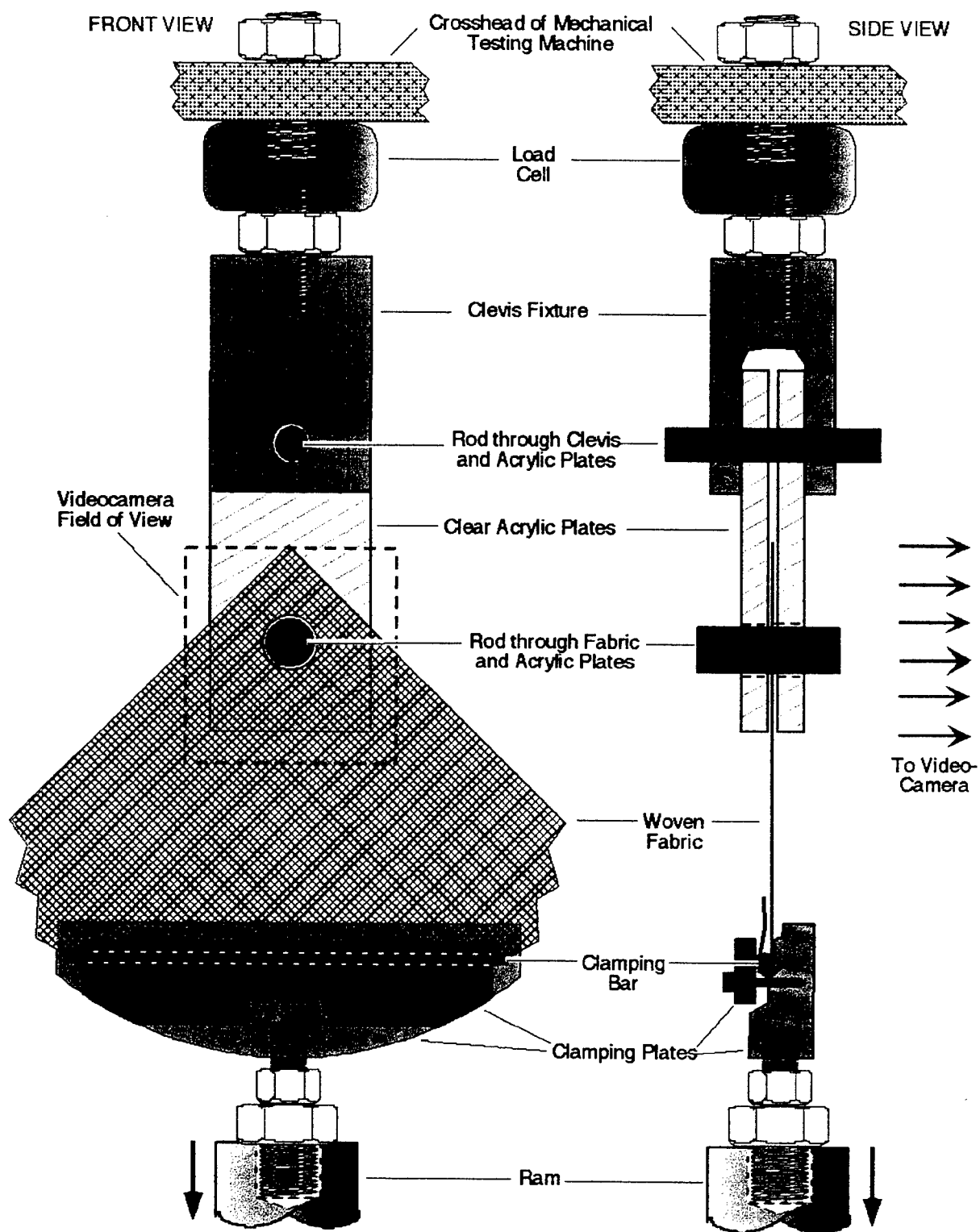- Clamping Plates
- Ram

FIGURE 17. EXPERIMENTAL DESIGN FOR FABRIC CORNER FAILURE TESTS

24

COMPUTATIONAL MODELING OF FABRIC BARRIERS

## DETAILED SIMULATION OF IMPACT OF FABRIC GRIPPED ON CORNERS.

An LS-DYNA3D simulation was performed using the detailed model to further investigate the effects of gripping on the ballistic response of Zylon fabric. The DYNA3D software code was developed by the Lawrence Livermore National Laboratory as a tool for simulating dynamic nonlinear events such as impact. LS-DYNA is a commercial product available from Livermore Software Technology Corporation. In previous simulations it was found that a fabric barrier gripped on two edges absorbs more kinetic energy than a barrier gripped on four edges. Gripping on four edges results in a large initial resisting force, but because the gripped yarns break, the resisting force does not remain as long. Gripping on two edges results in a longer duration of resistance, because the load taken by yarns that break is shed to adjacent unbroken yarns.

The current simulation involved gripping the fabric on corners only. As in previous simulations, the fabric modeled was a square patch of 25 x 25 yarns. At the corners, five yarns were held in each direction. As shown in figure 18(a), the fabric was impacted with a 120-m/s fragment aligned over a 2 x 2 yarn square in the center of the fabric. Thus, none of the yarns that were directly hit with the fragment were gripped. It was expected that this method of gripping would result in fewer broken yarns and a longer duration-resisting load.

In this simulation, the fragment was stopped and thrown back. Results of the simulation are shown in figure 18. The figure shows the calculated response of the impacted fabric at three different times during the calculation. Figure 18(a) shows the initial configuration with the fragment just impacting the fabric. Figure 18(b) shows the response of the fabric at 40 μs. Because only the corners are held, the deformation under the fragment is considerable and the yarns along the edges begin to become detached. Figure 18(c) shows the simulation at 90 μs, the time at which the maximum deformation occurs.

Figure 19 shows the calculated velocity histories of the fragment for the corner-held simulation and for the simulation gripped on two edges. Initially, the fabric gripped on the corners slows the fragment more gradually than the fabric gripped on two edges; but by 50 μs, the corner-held fabric slows the fragment more quickly. By 50 μs, the held yarns that were impacted for the two-edge-gripped case have broken. As seen in figure 19, gripping the fabric on the corners stops the fragment at about 90 μs, compared to 120 μs when the fabric is gripped on two edges.

Figure 20 shows the calculated displacements of the fragment for the two cases. At the time when the fragment is just stopped, the peak displacement of the fabric is slightly higher (0.72 cm vs. 0.66 cm) for the fabric gripped on the corners. These simulations confirm that fabric gripping is a key parameter for optimizing barrier design and suggest that it is advantageous to grip the fabric in such a way that the impacted yarns are not broken.
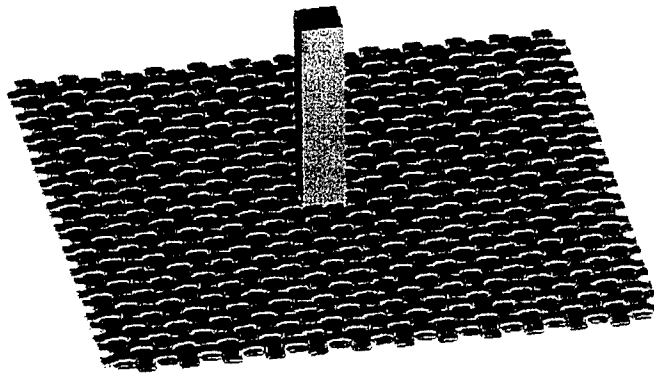
(a) Initial configuration
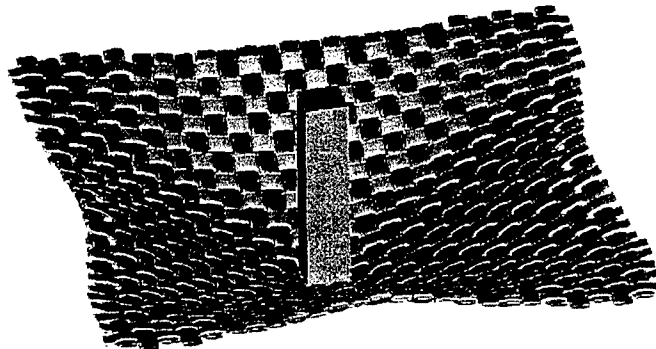
(b) Time = 40 μs
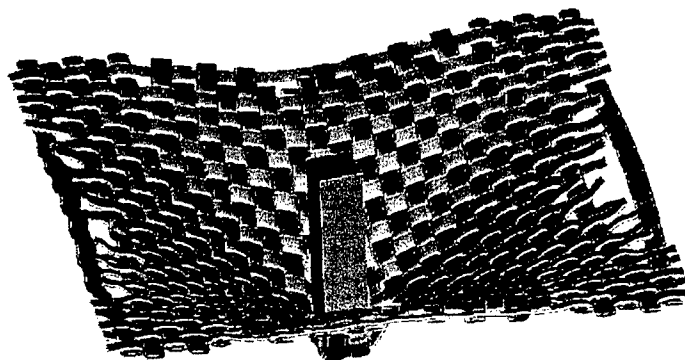
(c) Time = 90 μs

FIGURE 18. CALCULATED RESPONSE OF FABRIC HELD AT CORNERS

FIGURE 19. CALCULATED VELOCITIES FOR FABRIC GRIPPED ON
CORNERS AND GRIPPED ON TWO SIDES

FIGURE 20. CALCULATED DISPLACEMENTS FOR FABRIC
IMPACT SIMULATIONS

DESIGN MODEL CALCULATIONS OF LARGE-SCALE TESTS.

As described in previous reports, a simplified model is being developed that can be used as a design tool for choosing or evaluating parameters for fragment barriers. The design tool uses a continuum description of the fabric, 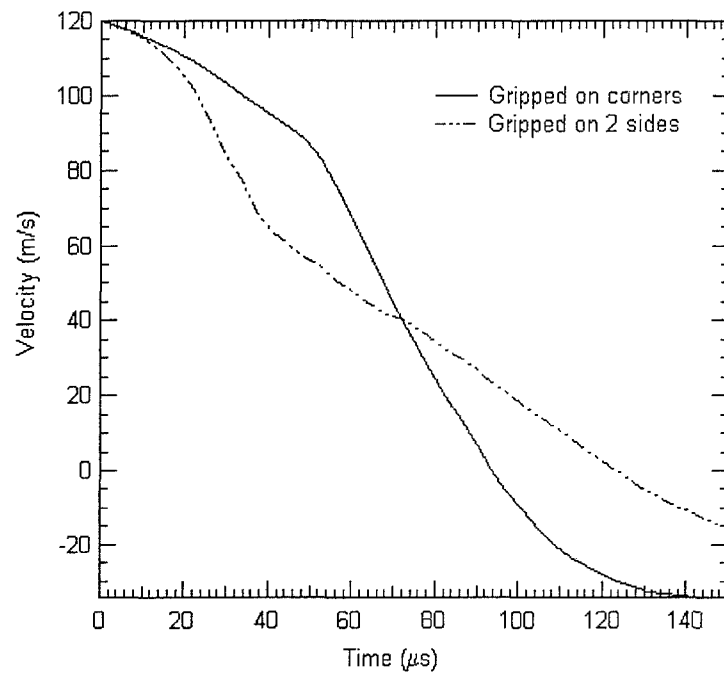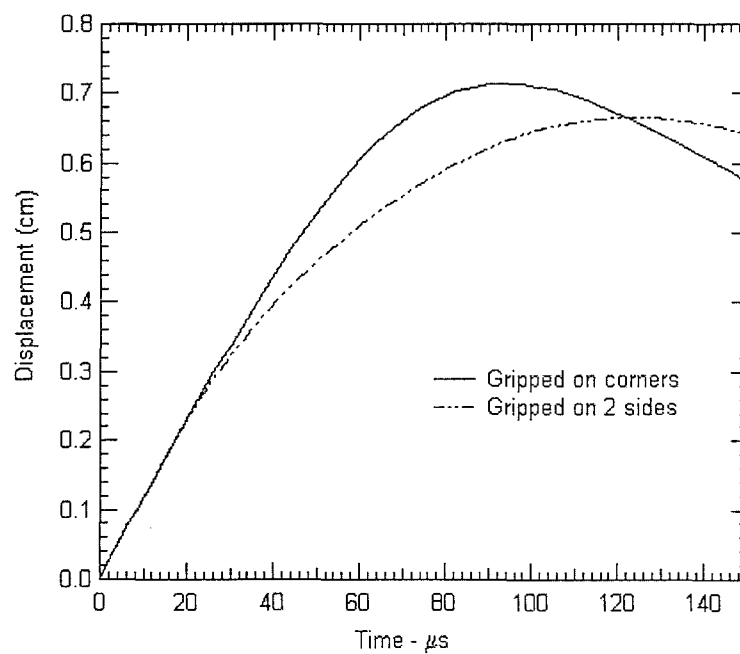and the calculations run quickly (about 5 minutes for a 1000-element simulation of a gas-gun test on a four-processor SGI Origin 200) and easily, allowing evaluation of the changes in fabric size, number of layers, or yarn pitch. The design model uses shell elements with an orthotropic continuum formulation to model the fabric.

Simulations were performed on the large-scale tests described above. These tests were performed, as shown in figure 6, using the 6-in.-bore gas-gun facility at CHES to investigate fundamental design variations for barriers including different strategies for attachment of fabric to the frame, different number of fabric plies, and different fabric size and configuration.

The titanium alloy fragment used in these tests was 4.0 in. (10.2 cm) long by 3.0 in. (7.6 cm) wide, with a thickness of 0.25 in. (0.62 cm) that tapers from the mid-point down to 0.05 in. (0.13 cm) at the impact end, where the edges are slightly rounded. The fragment weighed roughly 0.4 lb (175 g). The fragment impacts the fabric head-on with 0° obliquity and a 45° roll.

SIMULATION OF TEST 101. Figures 21 and 22 show the model configuration for a simulation of large-scale test 101. This test had three layers of Zylon and an impact velocity for the fragment of 230 m/s. The attachments were modeled explicitly by including a hole in the fabric and a 1-in.-diameter bolt with a 2-in.-diameter flat head top and bottom. In this view, the fragment starts below the fabric and travels upward. The fabric has been made translucent in this figure to show the motion of the fragment. The sag in the fabric, required to fit the barrier around the insulation package within the fuselage section, is approximately 5 in. (12.7 cm) deep on one end and 7 in. (17.8 cm) deep on the other. The fragment is rotated with a 45° roll angle. The color fringes of the fragment correspond to the magnitude of the velocity in the z direction.
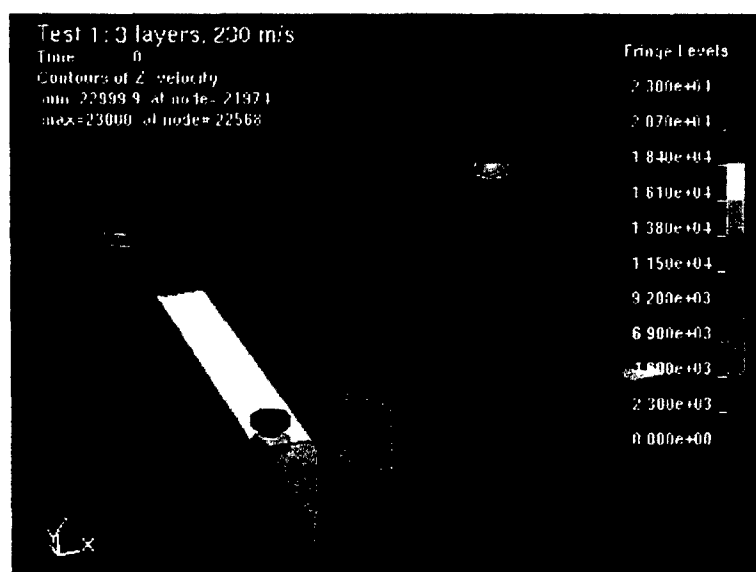

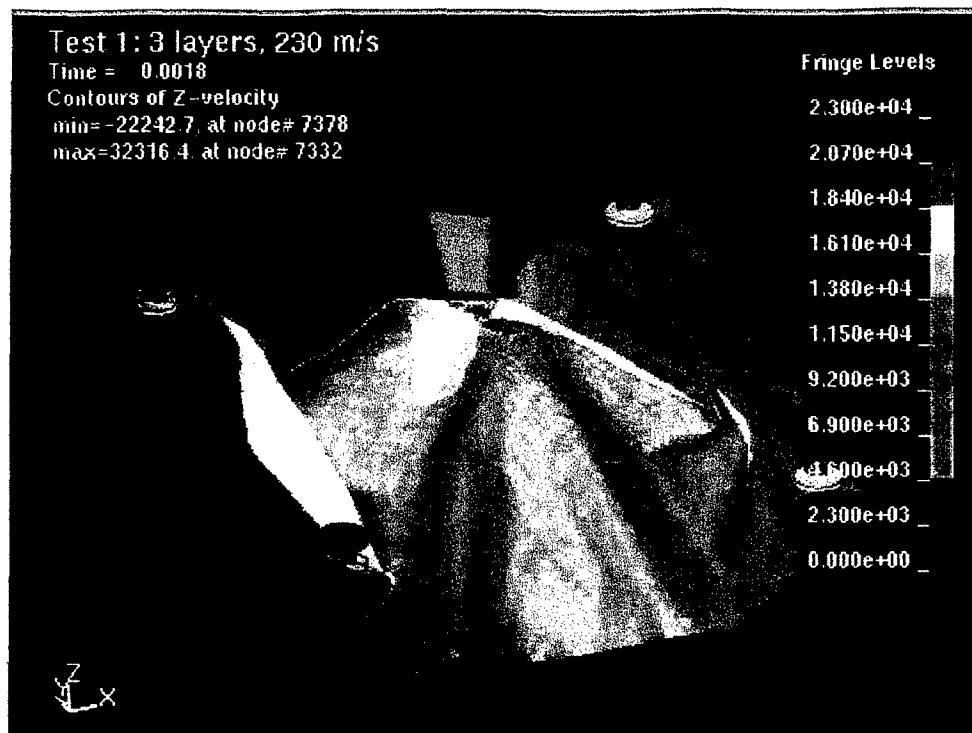FIGURE 21. SIMULATION MODEL FOR TEST 101

FIGURE 22. SIMULATION OF TEST 101 AT 1.8 ms
(Fragment impacting from bottom to top)

Figure 22 shows the simulation at a time of 1.8 ms. By this time, the fragment has completely penetrated the fabric. As seen by the deformation of the fabric, the fragment penetration occurs before the fabric has completely stretched out. The calculated residual velocity of the fragment was 180 m/s and the measured value was 202 m/s, thus the model is too strong in this case. An animation of this simulation can be viewed on the project web site at http://www.sri.com/poulter/ air_safety/design_model.html.

SIMULATION OF TEST 114. Simulation results for large-scale test 114 are shown in figure 23. Compared to test 101, test 114 was a larger target and had no sag in the fabric. In this figure, the fragment is traveling left to right, and the fabric was made transparent so the fragment could be seen. At 1 ms, the fragment velocity was 100 m/s; at 2 ms, the velocity was 55 m/s; and at 3 ms, the fragment had penetrated the fabric with a residual velocity of 20 m/s. The residual velocity measured in the experiment was 83 m/s. Similar to the simulation of test 101, the model is too strong. In terms of energy, the model overpredicts the energy absorbed by 0.58 kJ. Preliminary investigation of the deformation of the fabric shows that the model is too stiff (i.e., the simulation shows less deformation of the fabric than seen in the experiment).

(a) t = 1 ms   (b) t = 2 ms   (c) t = 3 ms
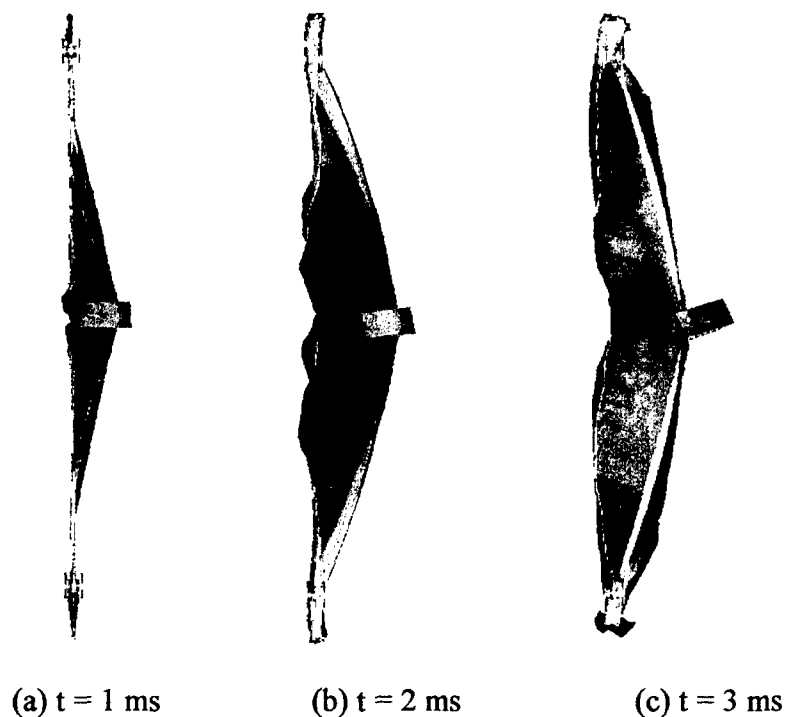
FIGURE 23. SIMULATION OF TEST 114

DISCUSSION OF LARGE-SCALE SIMULATION RESULTS.   Simulations were also performed for tests 106 through 110 in addition to tests 101 and 114. In all of these tests, the fabric target broke at one or more of the attachments. In these simulations, the fragment did not penetrate the fabric for any of the test configurations. In the experiments, the fragment penetrated for tests 106, 107, and 109. Figure 24 shows the model's results from test 107. In this simulation, the fabric effectively resists penetration because it tumbles the fragment. Because the failure criterion for the model requires yarns in two directions to fail, the corners in the simulation did not fail.

FIGURE 24. SIMULATION OF TEST 107

30

In all the simulations performed for the large-scale tests, the model was too strong and too stiff. The constants used for the model were those determined from the small-scale gas-gun tests performed at SRI International. For those tests, measurements were not taken of the fabric deformations during fragment impact, therefore, the design model could not be verified for stiffness. There were only a few tests with multiple plies of fabric. For the large-scale tests, however, good records exist for the deformation, and all the tests had at least two plies of Zylon. The large-scale test data will be used to improve the Zylon model response for both stiffness and deformation (see Future Plans section).

DEVELOPMENT OF LINUX CLUSTER.

Until now, all the simulations for both the detailed and design model have been run on a four-processor SGI Origin-200. This computer is limited in its capacity to run large simulations. Calculation of the detailed model for a 25 x 25 yarn patch of fabric takes about 8 hours on this computer. To increase the size of the fabric patch that can be simulated using the detailed model, a PC cluster that runs a shared memory parallel version of LS-DYNA simulations is being developed. The cluster, supplied by SGI, is six PC boxes, each with two 733-MHz Pentium III processors (12 processors total) linked by T10/100 Internet connections.

Although it is generally agreed that these cluster platforms are the best option for future technical computing, experience has shown that it still takes considerable development to achieve a working system because of the different hardware and software systems that need to work together. The hardware required includes several PCs with Internet connections and a hardware switch. The software must include a Linux operating system, message passing interface (MPI) software for running parallel jobs, C and Fortran compilers, and an MPP/Linux version of LS-DYNA. Because Linux and MPI are not standard, different versions of the software exist and incompatibilities between the software versions invariably arise. For example, LS-DYNA requires the LAM version of MPI libraries, but that was not the version shipped by SGI. Furthermore, differences in naming protocols between FORTRAN (e.g., two underscores following subroutine names rather than a single underscore) caused additional complications. A working version of LS-DYNA is now running on the SGI PC cluster, and trial simulations are under way to assess the computational capacity of the new system.

FUTURE PLANS

EXPERIMENTAL PHASE.

The following work is planned:

- A series of fabric corner failure tests are planned, as described at the end of the section on impact testing. The series will focus on the deformation and failure behavior of the fabric around pegged hole corners and will provide data needed for model refinement and verification. The results of these tests and the computational simulations will help determine corner holding designs to be used in further impact testing that allow for fabric deformation and failure in the corner regions, but do not allow complete corner failure (detachment from the frame).

- Another series of large-scale impact tests at SRI's remote test site is planned. Using the Unistrut mounting frame, these tests will focus on fabric barrier design variables needing further examination for model verification, fabric material (Kevlar as well as Zylon), number of plies, lateral fabric dimensions, and location of impact point (off-center on the barrier, as well as centered).

- Analysis of the cut resistance tests will be completed.

COMPUTATIONAL PHASE.

- The deformations of the fabric for the large-scale tests will be analyzed, and the results will be used to improve the stiffness and strength response for the Zylon model.

- Methods to model attachment failure will be investigated. In particular, the use of large strains in a single direction as a failure mode will be examined.

- A new PC cluster, configured to run LS-DYNA3D in an efficient manner, will be purchased by SRI and set up to perform the fabric model simulations.

REFERENCES

1. Aircraft Catastrophic Failure Prevention Research Program, Program Plan, January 1994, U.S. Department of Transportation, Federal Aviation Administration, Technical Center, Atlantic City International Airport, New Jersey, 1994.

2. D.A. Shockey, J.H. Giovanola, J.W. Simons, D.C. Erlich, R.W. Klopp, and S.R. Skaggs, "Advanced Armor Technology: Application Potential for Engine Fragment Barriers for Commercial Aircraft," DOT/FAA/AR-97/53, William J. Hughes Technical Center, Atlantic City International Airport, New Jersey, July 1997.

3. C.E. Frankenburger, III, "Large Engine Debris Analysis" DOT/FAA/AR-99/11, William J. Hughes Technical Center, Atlantic City International Airport, New Jersey, May 1999.

4. D.C. Erlich, D.A. Shockey, and J.W. Simons, "Improved Barriers to Turbine Engine Fragments: Interim Report III," DOT/FAA/AR-99/8,III, William J. Hughes Technical Center, Atlantic City International Airport, New Jersey, May 2001.

5. D.C. Erlich, D.A. Shockey, and J.W. Simons, "Full-Scale Tests of Lightweight Fragment Barriers on Commercial Aircraft," DOT/FAA/AR-99/71, William J. Hughes Technical Center, Atlantic City International Airport, New Jersey, July 1999.

APPENDIX A—EVALUATION OF CUT RESISTANCE IN HIGH-STRENGTH FABRICS

ABSTRACT.

To assist development of the computational fabric model, an experimental study of the cut resistance of fabric barrier materials was performed. Transverse cut tests at various angles of cutter blade inclination were performed on Zylon, Kevlar, and Spectra yarns to measure their response and to investigate the failure mechanism involved in the cutting process. In tests with a utility blade (≈ 2 μm radius of curvature), Zylon required 4 times as much energy per linear density than other two materials, for cut-through at 0° angle of inclination. This fracture energy decreased sharply with increased inclination angle, as did the initiation strain for fiber failure. The effects of blade angle inclination, blade sharpness, and axial pre-tension in the yarn are presented.

INTRODUCTION AND BACKGROUND.

Previous work at SRI to characterize the fragment impact energy absorption capability of high-strength fabrics [A-1 and A-2] indicated that absorbed energy dropped significantly with the sharpness of the fragment's impact edge. It was also observed during sample preparation that the fabric's cutting resistance declined sharply with blade inclination angle. Therefore, an understanding of the failure behavior in the fabric under sharp edge loading over a range of blade inclination angles was considered important for calibrating the fabric computational models and improving the current capability for designing engine fragment barriers.

A literature search on measurement of the cut resistance of fabrics revealed some work on various protective clothing such as gloves, which had been done for the purpose of reducing industrial accidents [A-3 through A-6]. Some standard test methods had been established, but these tests provided only a relative comparison of the fabric's ability to resist cut-through in a particular geometry (against a rigid mandrel, for example) and do not provide a material property or governing mechanism that would be useful in more general applications, such as penetration barrier design. In one study [A-5], for example, no distinct correlation was found between a fabric's penetration resistance and its resistance to being cut by a reciprocating circular blade.

Generally, a fabric can be cut in the following three modes: (1) by transverse loading by a sharp blade (with or without a slicing component) against a rigid substrate, (2) by transverse loading by a sharp blade (with or without a slicing component) with no substrate, and (3) by simple shearing, as with a scissors.

High-strength fabrics make effective ballistic barriers because they can absorb a lot of energy through transverse fabric deflection and resultant yarn stretching, thereby spreading the concentrated load at the fragment impact region outward along the axial direction of the warp and fill yarns to encompass a larger area of the fabric. Only the second of the above three cutting modes loads the fabric in such a way as to cause significant transverse deflection prior to cutting. The transverse loading with no substrate mode was therefore selected for this study, as it was most relevant to ballistic barriers.

No standard test procedure exists for the transverse cutting of fabrics, and little work has been reported on transverse cut resistance. Since the cut resistance of fabrics depends on the interaction of yarns in the fabric [A-7], the first step is to investigate the cut resistance of individual yarns. Later work could then consider the cut resistance of woven fabrics. A limited study involving transverse cut resistance in Zylon and Kevlar yarns was performed previously in this Federal Aviation Administration (FAA) program [A-2], but those few tests involved only a single blade sharpness (≈ 20 µm radius of curvature), only 0° angle of blade inclination (therefore no slicing component), and no axial pre-tensions in the yarn.

The objectives of this work are to characterize the failure resistance of Zylon, Kevlar, and Spectra yarns subjected to transverse loading by a sharp blade and to determine the dominant failure mechanisms during the cutting process. Below in this appendix, the experimental technique is discussed in detail, followed by the experimental results obtained thus far. The influence of angle of blade inclination, blade sharpness, and axial pre-tensions on the yarn's cut resistance is presented. Finally, plans for completing the analysis during the next program year are outlined.

TRANSVERSE CUT TESTS—SETUP AND PROCEDURE.

FABRIC SPECIMENS. Three types of high strength fabrics—Zylon, Kevlar, and Spectra— were used in the cut resistance tests. Table A-1 shows the relevant properties of these fabrics.

TABLE A-1. PROPERTIES OF HIGH-STRENGTH FABRIC MATERIALS

Fabric Name[a]	Material	Volume Density (g/cm^3)	Mesh (yarns/in.)	Tensile Modulus (GPa)	Failure Strain (%)	Area of Cross Section $(in.^2)$
Zylon-AS	PBO	1.5	30 x 30	171	3.4	5.6575E-05
Kevlar-29	P-Aramid	1.4	32 x 32	104	3.3	4.8205E-05
Spectra-1000	UHMW Polyethylene	0.97	32 x 32	103	3.1	6.479E-05

[a] Zylon is a Toyobo registered trademark; Kevlar is a DuPont registered trademark; Spectra is an AlliedSignal registered trademark.

The fabric specimens were 5 in. wide and 12 in. long in the direction of fill yarns. As shown in figure A-1, they were tightly gripped at two edges in the fabric-holding fixture previously used for the yarn pullout tests [A-2]. The fabric length between grips (i.e., the yarn gauge length) was ≈ 6.5 in. To isolate individual fill yarns for testing (to avoid any contact between the blade and adjacent yarns), the fill yarns between the isolated fills to be tested were removed, along with all of the warp yarns, in the region between the grips. Each fabric sample had approximately six isolated fill yarns with a space of 0.5 in. between them. At both edges of the sample, 15 fill yarns remained to keep the sample aligned during mounting and testing.
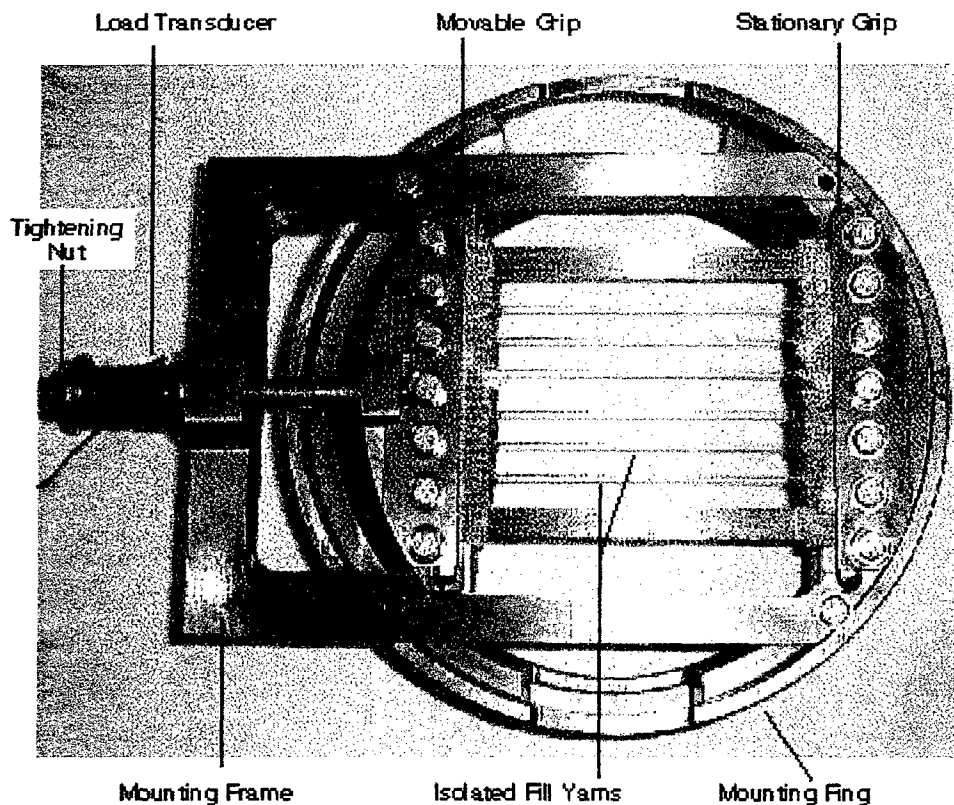
FIGURE A-1. ZYLON FABRIC SPECIMEN WITH ISOLATED FILL YARNS
PREPARED FOR TRANSVERSE CUT TESTS

The sample holding fixture has one movable grip and one fixed grip, so it was possible to apply a pre-tension to the yarns by tightening the nut attached to the movable grip. A load transducer placed between the nut and the frame measured the total axial pre-load on the fabric specimen, divided by the number of uncut fill yarns to determine the axial pre-load on the specimen yarn.

CUTTER BLADES. The sharpness of the cutter blade is a critical variable for cut resistance testing. It is important that the blade be sharpened to a consistent level before each test. To achieve this, a commercially available, hardened steel utility blade[*] with a 30° included angle and an edge radius of curvature of ≈2 μm was selected as the baseline cutting edge. This blade was referred to as the "utility blade." Figure A-2 shows Scanning Electron Microscope (SEM) views of a virgin utility blade and one that had been used in a transverse cut test with a Zylon yarn. The virgin blade does show some slight irregularities in its cutting edge, but they are less than the ≈12-μm diameter of the Zylon fibers. The used blade shows evidence of significant edge deformation and blunting. A new blade was therefore used for each cut test.

A hardened steel panel machined to a 45° included angle and an edge radius of curvature of ≈20 μm (used in the previously reported transverse load tests [A-2]), was selected as the contrasting edge for blade sharpness comparison studies. This blade was referred to as the "machined edge."

_____

[*] 11-921 heavy duty utility blade, manufactured by Stanley Tools, New Britain, CT 06050.

TEST PROCEDURE. Figure A-3 shows the experimental setup for the yarn transverse cut tests. The fabric sample with the isolated fill yarns was mounted horizontally in a frame, which was affixed atop the ram of the MTS servo-hydraulic mechanical testing machine. The cutter blade was held above the fabric and attached to the crosshead of the MTS machine through a load cell, which measured the load on the cutter (or the transverse load on the mid-point of the yarn). The blade was attached at different angles of inclination (0°, 7.5°, 15°, 30°, or 45°) with respect to the plane of the fabric. The upward movement of the ram (at a constant ram rate of 0.01 in./s) pushed the yarn up against the cutter blade. The ram stroke (which equals the deflection of the yarn mid-point only for a 0° blade inclination angle, for which there is no slip of the yarn along the blade edge) and the transverse load on the yarn mid-point were recorded continuously throughout the test.
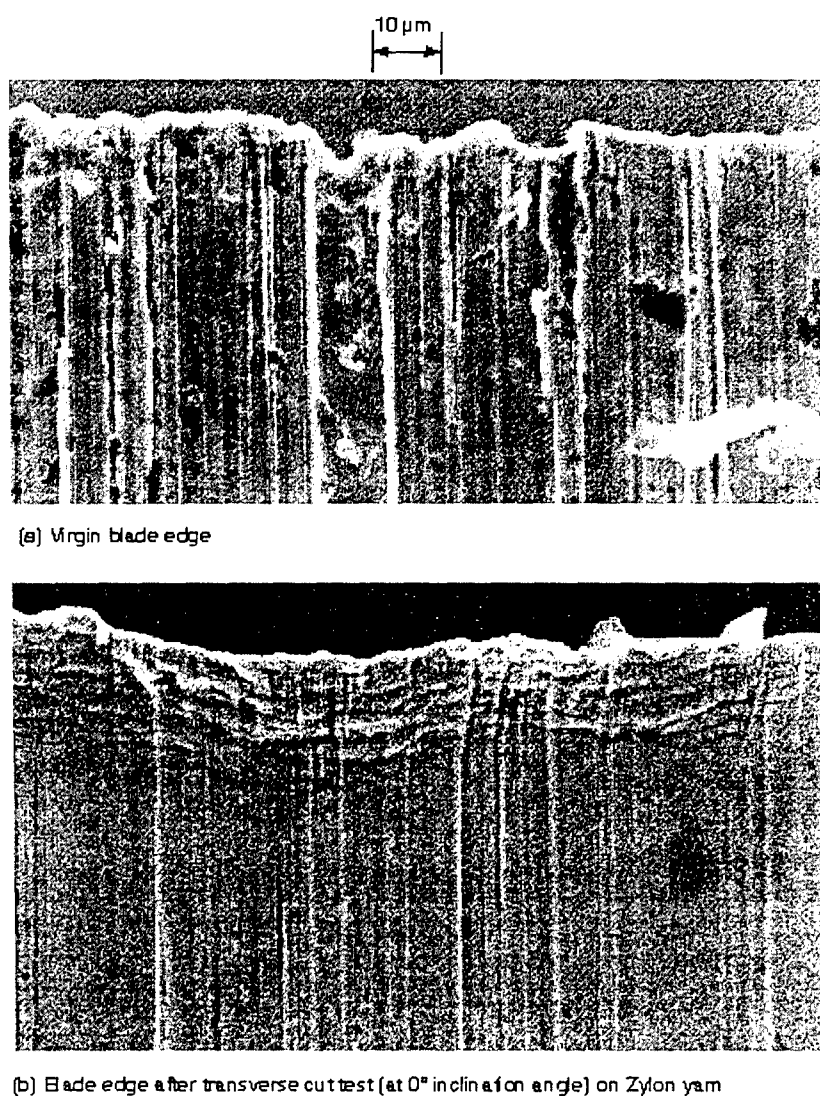

(a) Virgin blade edge

(b) Blade edge after transverse cut test (at 0° inclination angle) on Zylon yarn

FIGURE A-2. DEFORMATION IN THE CUTTING EDGE OF A UTILITY
BLADE FROM USE IN A TRANSVERSE CUT TEST

A-4

(a) Front View

Crosshead of Mechanical Testing Machine

Load Cell

Load Transducer — Aluminum Tube with Four Strain Gauges around Periphery

Blade Holding Fixture

Cutter Blade

Clamping Plate

Clamping frame

Scale

Fabric Sample

Clamping Bar

Movable Grip

Port in Mounting Ring

Stationary Grip

Clamping Bar

Nut — Applies Axial Pre-tension

Mounting Ring

Bracket

Ram

(b) Side View

Load Cell

Crosshead of Mechanical Testing Machine

Blade Holding Fixture

Clamping Plate

Cutter Blade

Clamping Bar

Scale

Angle of Inclination

Clamping frame

Port in Mounting Ring

Mounting Ring
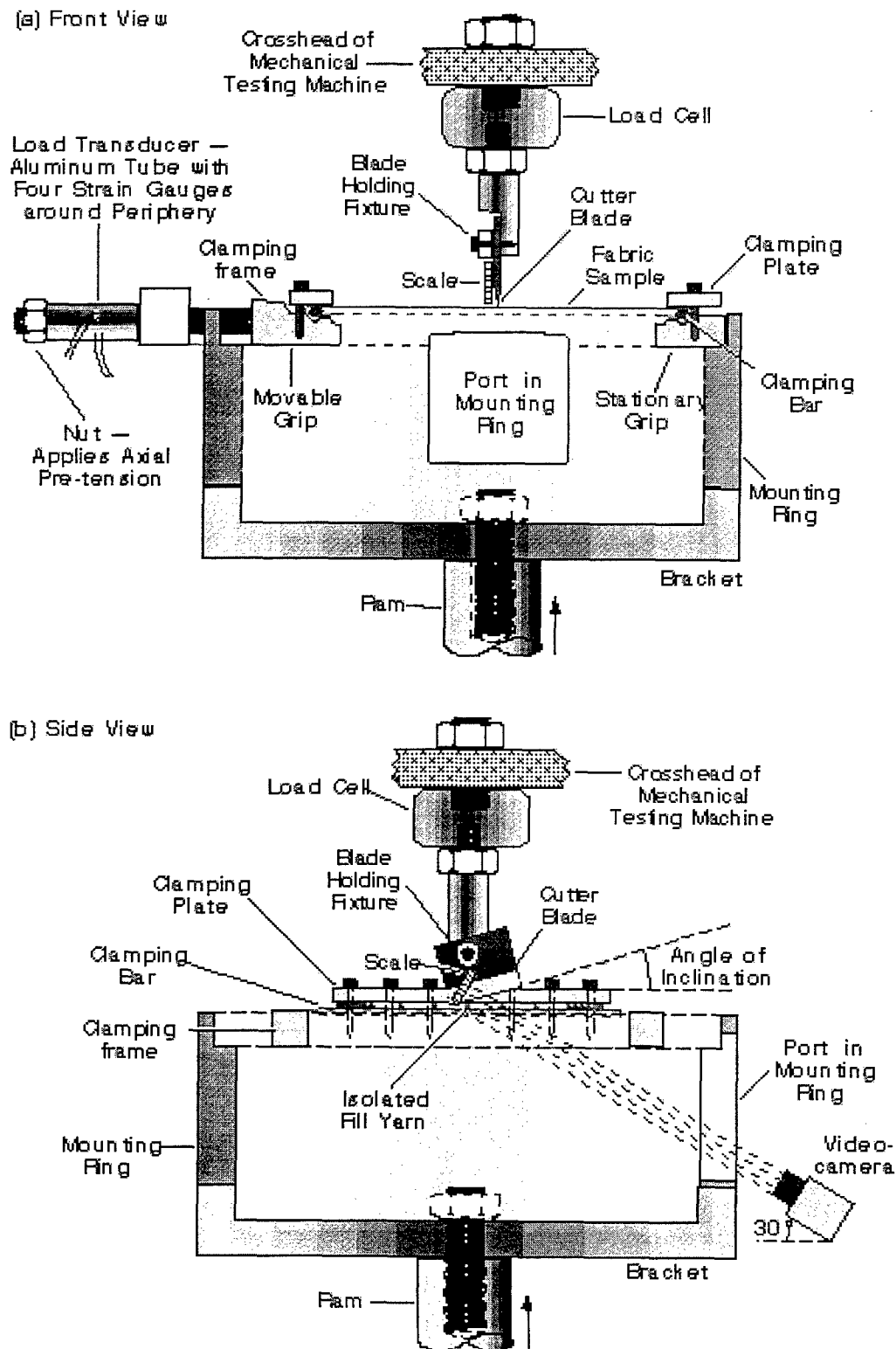
Isolated Fill Yarn

Video-camera

30°

Bracket

Ram

FIGURE A-3. SETUP FOR YARN TRANSVERSE CUT TESTS

A Charge Coupled Device (CCD) video camera was used to determine the instants of blade-yarn contact and initial fiber breakage and to observe the failure behavior. It also recorded the slippage of the yarn along the edge of the blade for tests with non-zero inclined angles, providing data needed for determining the stress and strain in the yarn for those tests. The camera was oriented at an angle of 30° with respect to the fabric plane, and a scale bar was attached to the cutter at right angles to the direction of the camera to assist in determining the yarn slippage.

The geometry for the stress-strain analysis for the transverse cut tests is shown in figure A-4. The strain in the yarn was calculated from the transverse deflection of the yarn. The stress was calculated from the axial load on the yarn, which is derived from the measured transverse load and the angle of yarn deflection.

For the case of 0° blade inclination (figure A-4(a)), for which no yarn slippage along the blade can occur, the yarn elongation, L, the induced strain, ε, and the angle of yarn deflection, θ, were determined simply by

$$L = 2 \left[(L_0/2)^2 + d^2 \right]^{1/2}, \tag{A-1}$$

$$\varepsilon = (L - L_0) / L_0, \tag{A-2}$$

$$\theta = \arctan (d / L_0), \tag{A-3}$$

where L_0 is the initial gauge length between grips, and d is the ram deflection (which equals the actual deflection of the yarn's mid-point). The axial force along the yarn (F_y) is determined from the measured transverse load (F) by

$$F_y = F / (2 \sin \theta), \tag{A-4}$$

and the stress, σ, is given by

$$\sigma = F_y / A, \tag{A-5}$$

where A is the yarn's cross-sectional area.

For the more general case of a blade angle of inclination α, the slippage of the yarn along the blade must be taken into consideration (see figures A-4b and A-4c). The video camera record shows the distance of slippage, S_P, as projected onto the scale. The actual slip along the blade, S, can be determined from
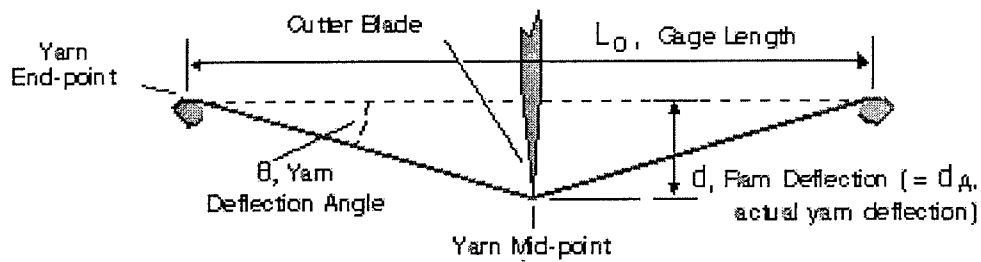
$$S = S_P / (\cos \beta), \tag{A-6}$$

where $\beta = 60 - \alpha$. The actual yarn deflection, d_A, can be then be derived, using the cosine theorem, from

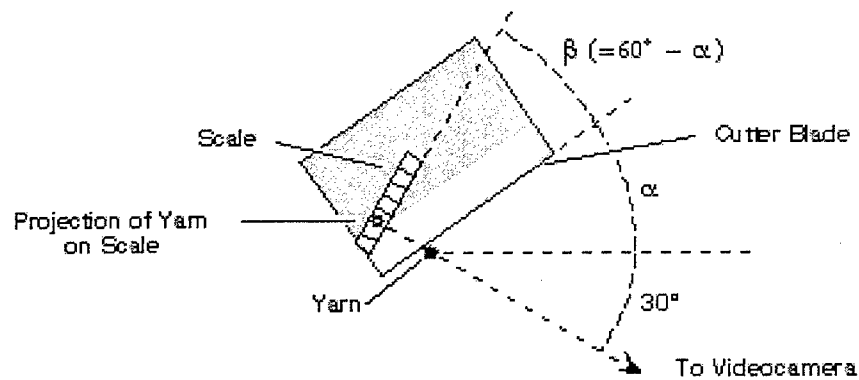$$d_A = \left[d^2 + S^2 - 2 d S \cos (90° - \alpha) \right]^{1/2}. \tag{A-7}$$

Then, the yarn strains and stresses can be derived by substituting d_A for d in equations A-1 and A-3, and then solving equations A-2, A-4, and A-5.

(a) Front view after ram deflection d, with 0° angle of inclination

Cutter Blade
L_0, Gage Length
Yarn End-point
θ, Yarn Deflection Angle
Yarn Mid-point
d, Ram Deflection (= d_A, actual yarn deflection)

(b) Side view at instant of contact, with angle of inclination α

β (=60° − α)
Scale
Cutter Blade
Projection of Yarn on Scale
α
Yarn
30°
To Videocamera

(c) Side view after ram deflection, d, resulting in yarn slide along blade, S

Yarn End-point
d
d_A, Actual Yarn Deflection
Projected Slide Seen by Video-camera on Scale
S_p
Yarn Mid-point
90°−α
S, Slide Along Blade (= S_p /cos β)
To Videocamera
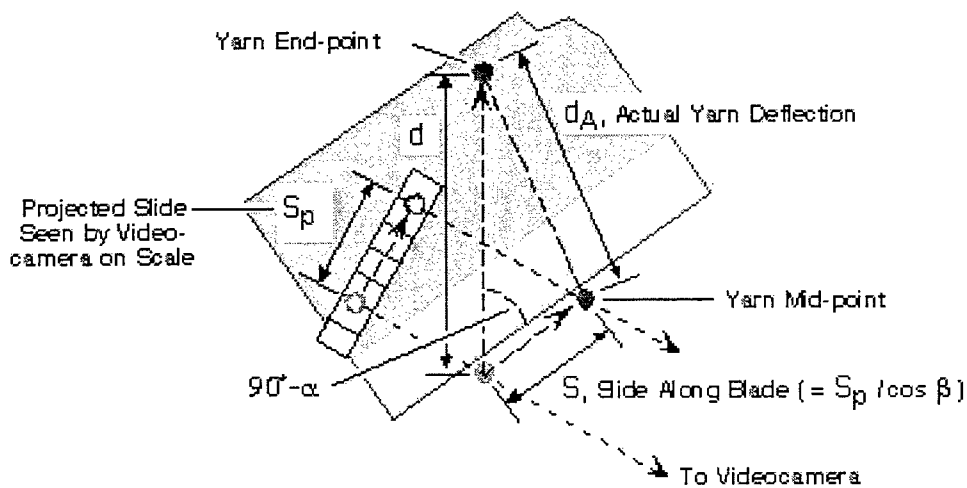
FIGURE A-4. GEOMETRY FOR STRAIIN ANALYSIS OF TRANSVERSE CUT TESTS

TEST RESULTS.

LOAD STROKE CURVES. A typical transverse load-stroke curve, obtained from a transverse cut test of a Zylon yarn with the utility blade at a 30° inclination and no pre-load, is shown in figure A-5. Also shown are four images from the video camera record, which depict: (a) the instant of blade contact with the yarn, (b) the initial fiber breakage, (c) the peak transverse load, and (d) a late stage of the test, along with their location on the load-stroke curve. Also, by noting the locations of the mid-point of the yarn, with respect to the scale on the four images, and comparing with the location of the arrow representing the initial contact location, one can determine the amount of slip during the test (roughly 0.1 in., which is not insignificant when compared with the total stroke of ≈0.6 in.).
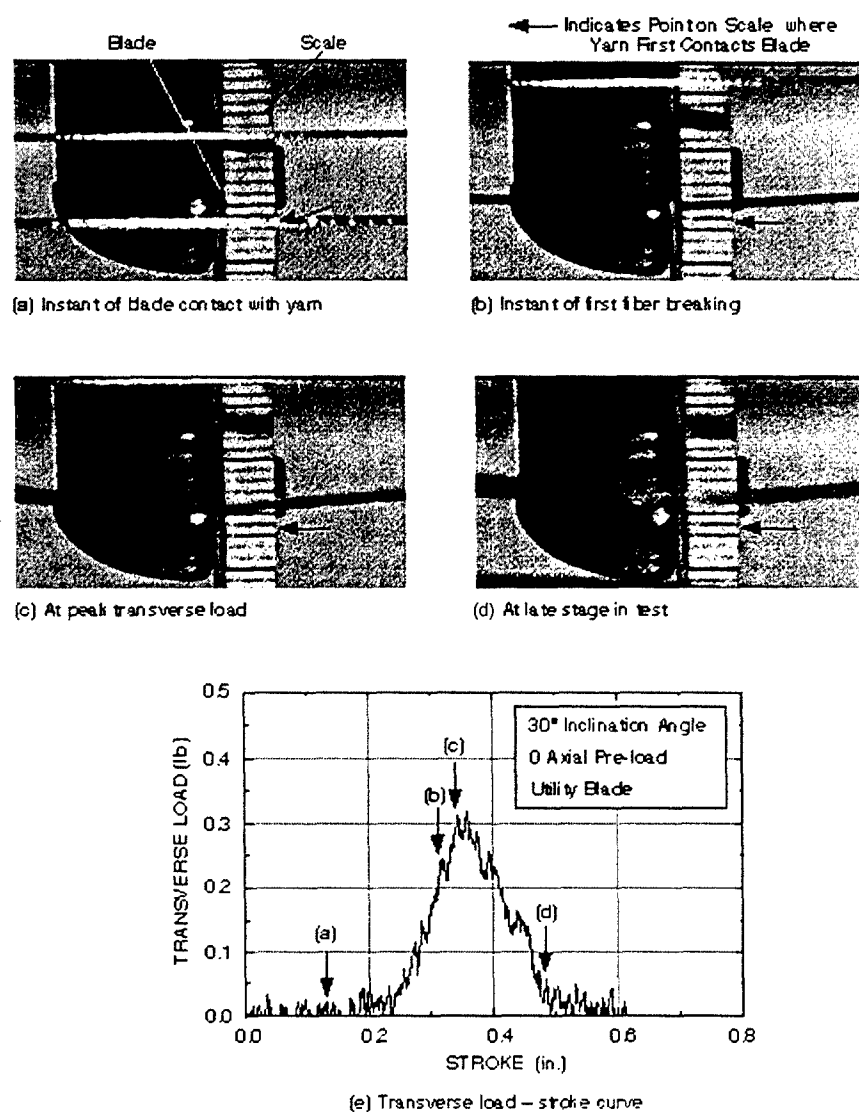
Blade   Scale

◄— Indicates Point on Scale where
     Yarn First Contacts Blade

(a) Instant of Blade contact with yarn

(b) Instant of first fiber breaking

(c) At peak transverse load

(d) At late stage in test

(e) Transverse load – stroke curve

FIGURE A-5. VIDEO IMAGES AT FOUR STAGES IN A ZYLON TRANSVERSE CUT
TEST AND CORRESPONDING LOCATIONS ON THE LOAD STROKE CURVE

A-8

The transverse load-stroke curves obtained for the three fabric materials at the various angles of inclination are shown in figure A-6. For Zylon* and Spectra yarns, the load continued to increase along a reduced slope after initial fiber breakage, and there was a gradual decrease in load after the peak. For Kevlar, however, the load increased steadily until a sudden burst of multiple fiber breakage caused a precipitous drop to nearly zero. For all three materials, the load-stroke curves for tests with inclined angles initially coincided with the curves for the 0° inclination tests, but deviated from those curves after the initiation of fiber breaking, which occurred at lower strokes for higher inclination angles.
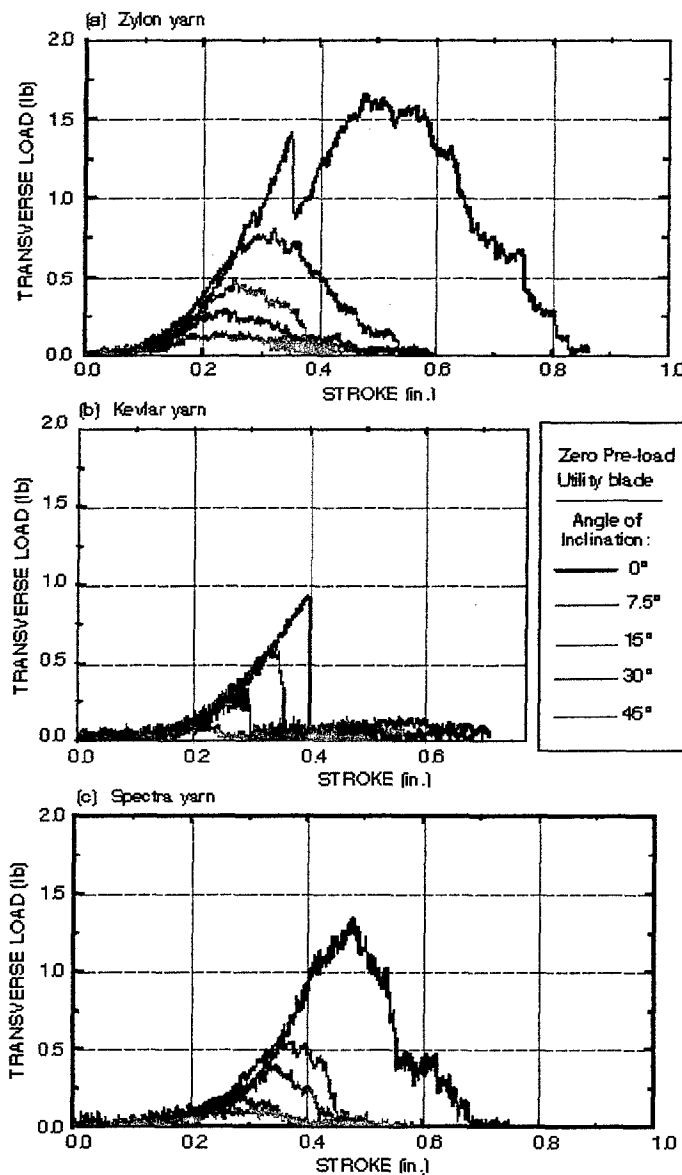
FIGURE A-6. LOAD-STROKE CURVES FROM TRANSVERSE CUT TESTS WITH THE UTILITY BLADE

---

* Sometimes for Zylon, a discontinuity on the load-stroke curve was observed after the initial (or other early) instance of fiber failure. It is thought that this may be due to a sudden change in the configuration of the fibers in contact with the blade.

FRACTURE ENERGY. The area under the transverse load-stroke curve equals the fracture energy; i.e., the energy required to deform and then break the yarn. For Zylon and Spectra yarns, a large fraction of the fracture energy was absorbed after the initial fiber breakage, but for Kevlar yarns, nearly all of the fracture energy was absorbed before the initial fiber breakage. Figure A-7(a) shows the average fracture energies obtained for the transverse cut tests at the different blade inclination angles. Fracture energies at $0°$ inclination angle were 0.93, 0.16, and 0.21 in-lb for Zylon, Kevlar, and Spectra yarns, respectively. The fracture energy decreased drastically as the angle of inclination increased, because of earlier fiber breakage, a reduction in peak load, and complete yarn failure at a smaller stroke.

Fracture energy per linear density is a useful parameter for comparing the cut resistance for yarns with different densities and cross-sectional areas. Figure A-7(b) shows the fracture energies per linear density obtained for the three different yarns at the five different angles of inclination. At $0°$, the value for Zylon is nearly four times higher than that of the other two materials. The value for Zylon decreases rapidly as a function of the inclined angle ($\approx 75\%$ drop at $7.5°$), more rapidly than the values for Kevlar and Spectra, but still exceeds the other two materials slightly at the highest angles. This dependency of fracture energy per linear density on the angle of inclination can be seen more clearly in figure A-8, which plots the energies per linear density for all of the yarns normalized to their values at $0°$.

TENSILE STRESS-STRAIN RELATIONS. Stress-strain relations during the transverse cut tests were derived from the transverse load-stroke data in the manner described above. For the cases of inclined angles, the slippage of the yarn along the blade edge needed to be taken into consideration. Results for a series of tests using the utility blade were shown in figure A-9. The points corresponding to the initiation of fiber breakage, as determined by the video camera records, are indicated by the arrow on each curve. For each material, the stress-strain curves for all angles nearly coincide until fiber breakage initiates, and the strain at which this occurs decreases as the inclination angle increases.

A series of transverse cut tests with the machined edge showed results similar to those with the cutter blade (figure A-10), except that the increased radius of curvature of the blade (e.g., decreased cutter sharpness) delayed the initiation of fiber breakage, leading to higher peak stresses and increased fracture energy. Figure A-11 compares the fracture energy for the two different blade sharpnesses. For each material, the fracture energy was significantly lower for the sharper blade. The effect was largest for Zylon and Spectra, where the difference between the two blades was nearly a factor of two or higher for all angles of inclination. Kevlar showed less difference ($\approx 30\%$ to 40%), at least for the two lowest inclination angles.
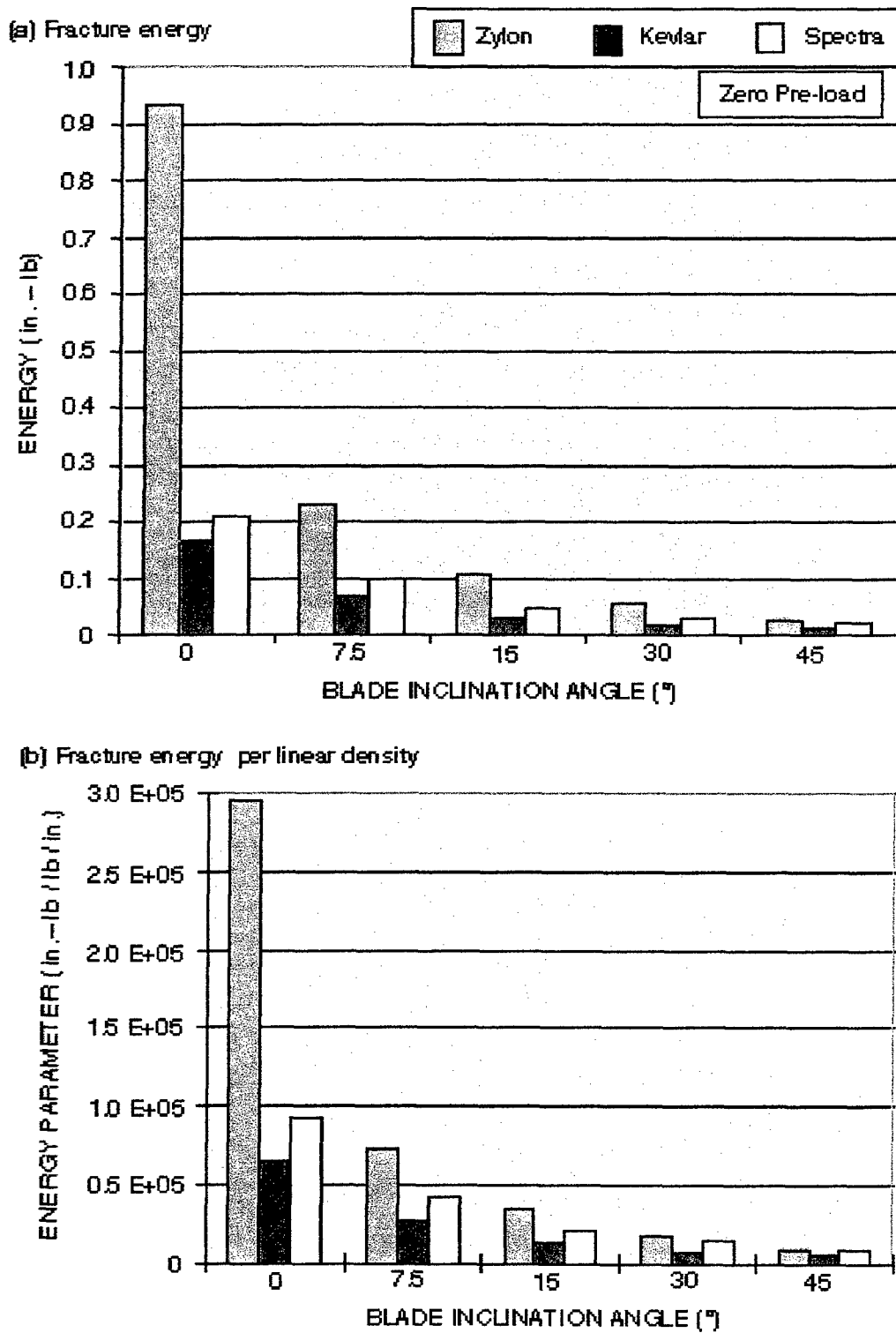
FIGURE A-7. DEPENDENCE OF FRACTURE ENERGY ON BLADE INCLINATION
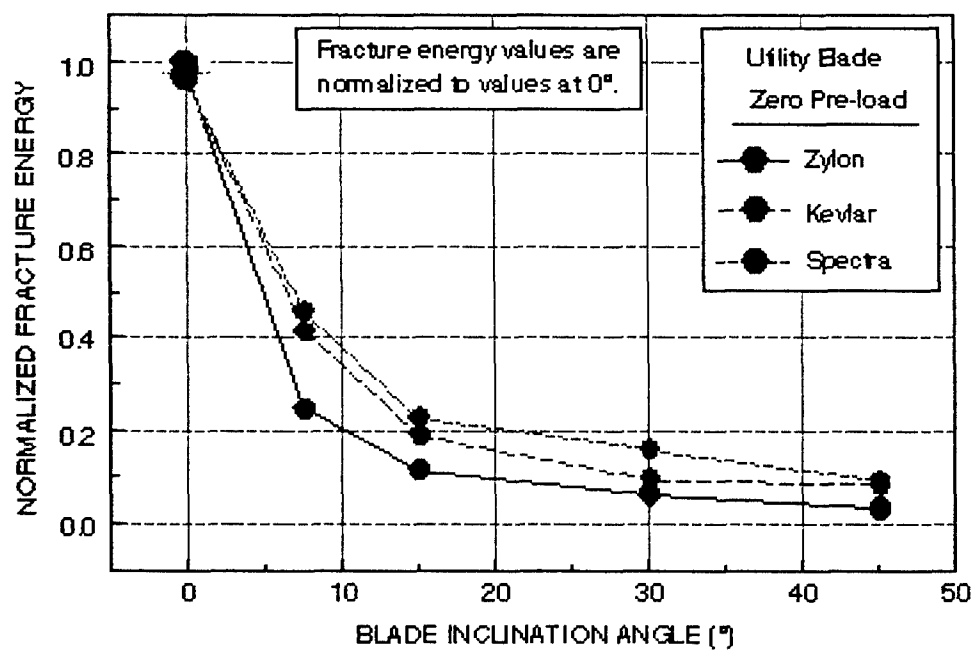ANGLE FOR TRANSVERSE CUT TESTS WITH UTILITY BLADE

FIGURE A-8. DEPENDENCE OF FRACTURE ENERGY UPON ANGLE OF BLADE
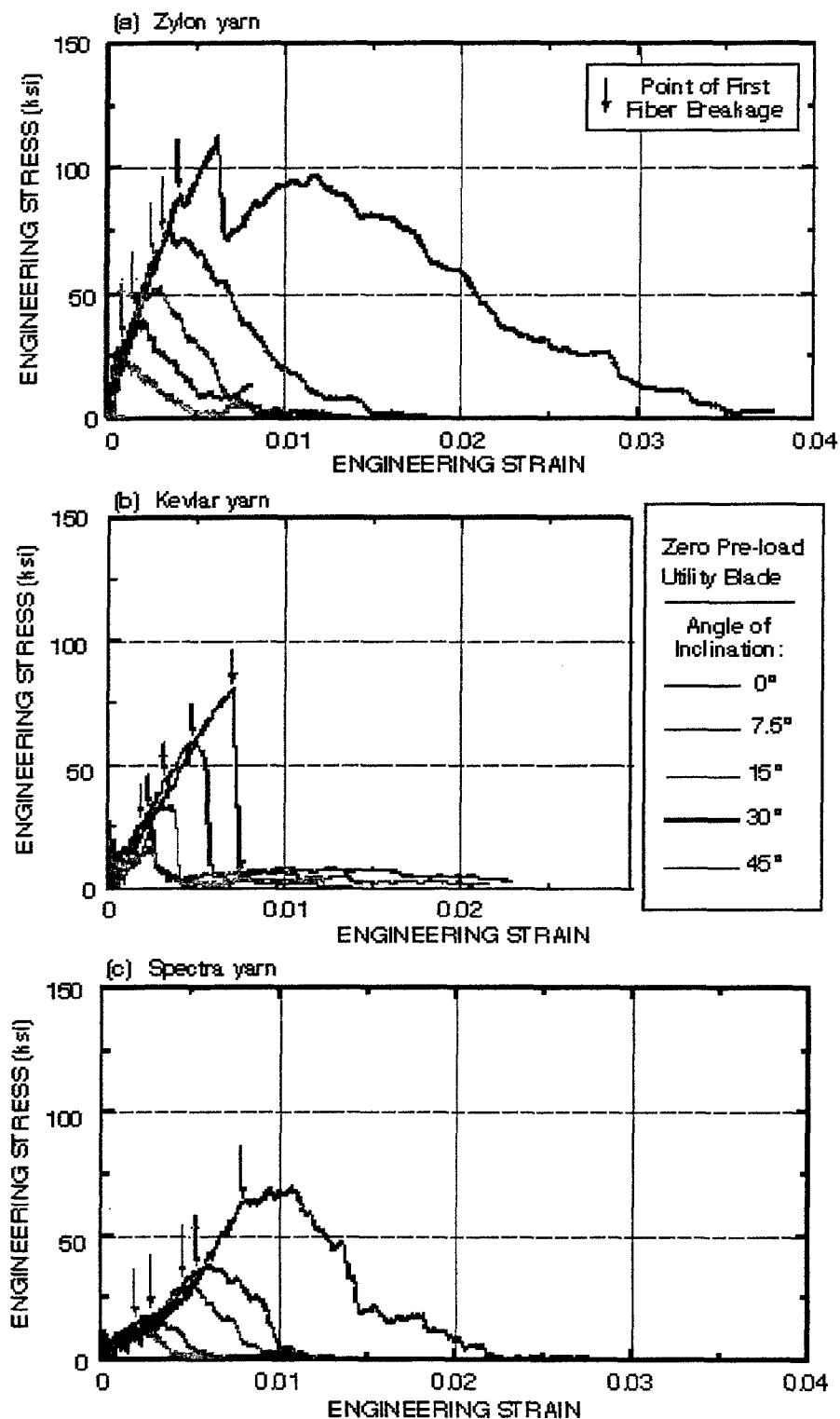INCLINATION IN THE TRANSVERSE CUT TESTS

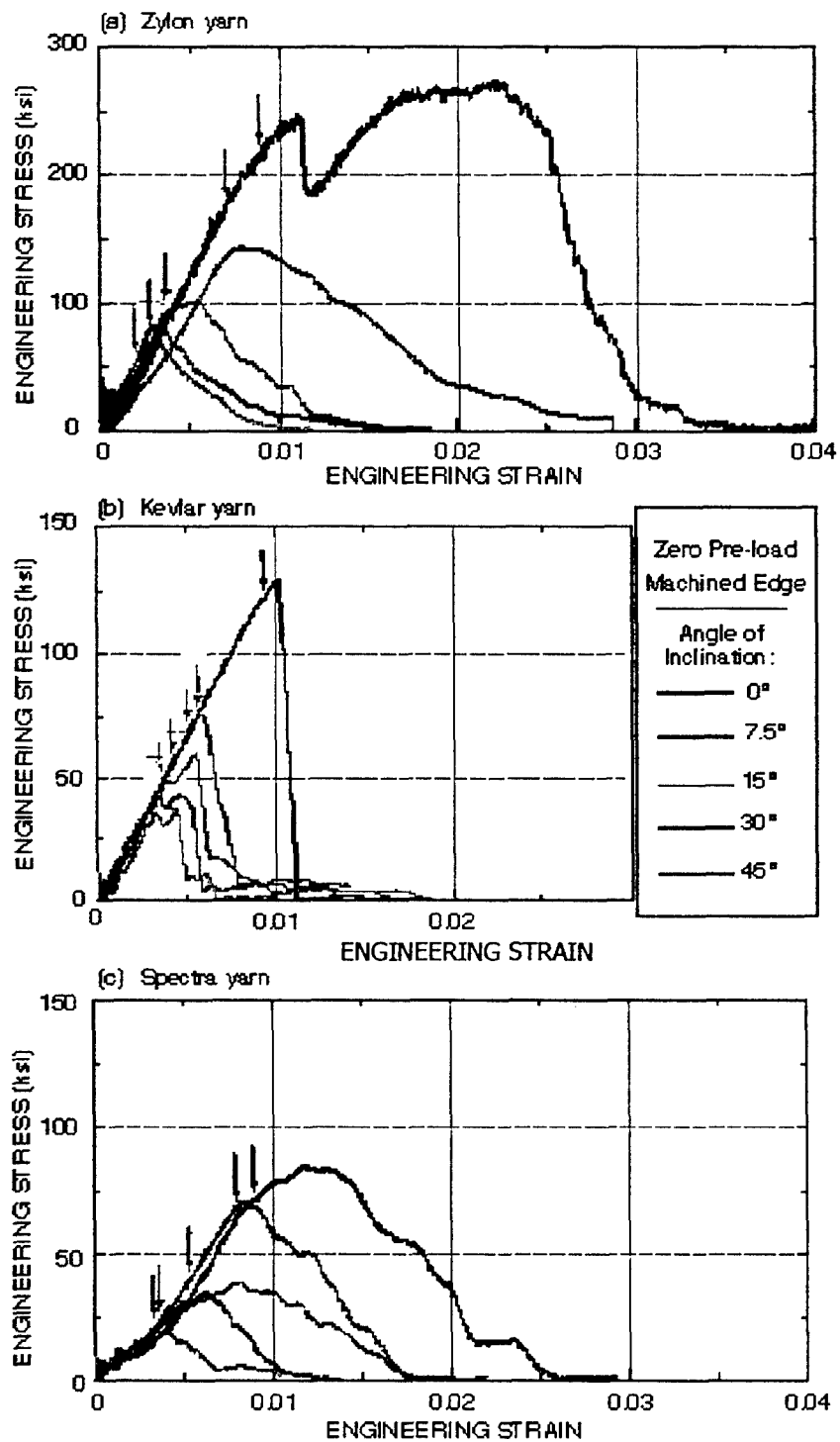FIGURE A-9. TENSILE STRESS-STRAIN CURVES FROM TRANSVERSE
CUT TESTS WITH UTILITY BLADE

FIGURE A-10. TENSILE STRESS-STRAIN CURVES FROM TRANSVERSE
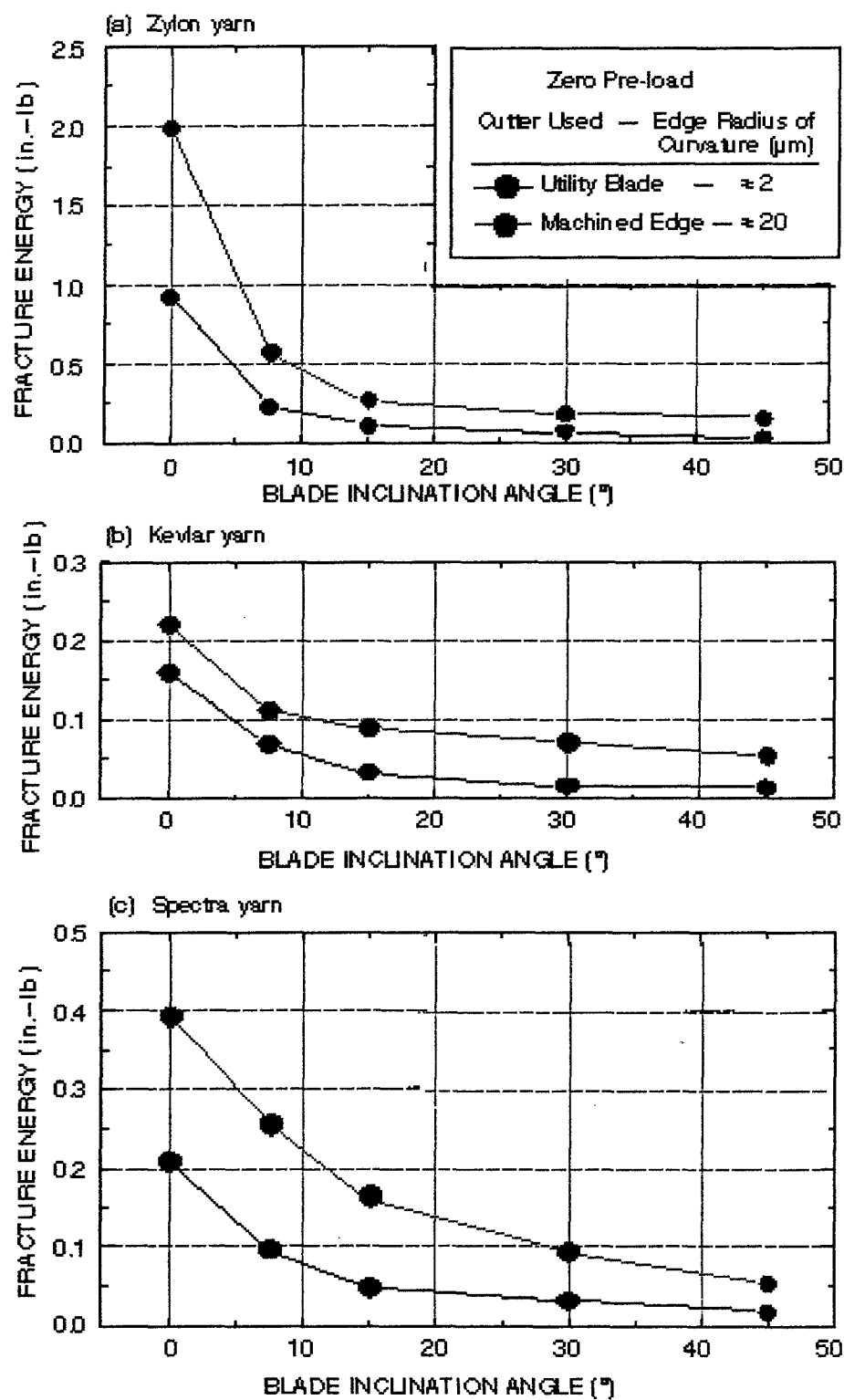CUT TESTS WITH MACHINED EDGE

A-14

FIGURE A-11. EFFECT OF CUTTER SHARPNESS ON FRACTURE ENERGY
IN TRANSFER CUT TESTS

In a fragment impact scenario, some plies in a fabric barrier (particularly plies toward the back of a multi-ply barrier) might be stretched and under significant tensile loads before the edge of a sharp fragment makes first contact. Therefore, it is important to understand how the cut resistance of a fabric might be affected by a tensile pre-load. Figures A-12 through A-14 show the effect of axial pre-tension on the yarn behavior during transverse cut tests. For each of the three materials, results of a test with the utility blade at a 0° inclination angle and no pre-load are compared with two similar tests with pre-loads that vary from 1 to 5 lb. As expected, pre-tension produced a shift in the transverse load-stroke toward lower stroke and load and an earlier fiber breakage initiation. Figure A-15 shows the decrease in the fracture energy for these tests as the pre-load increases.
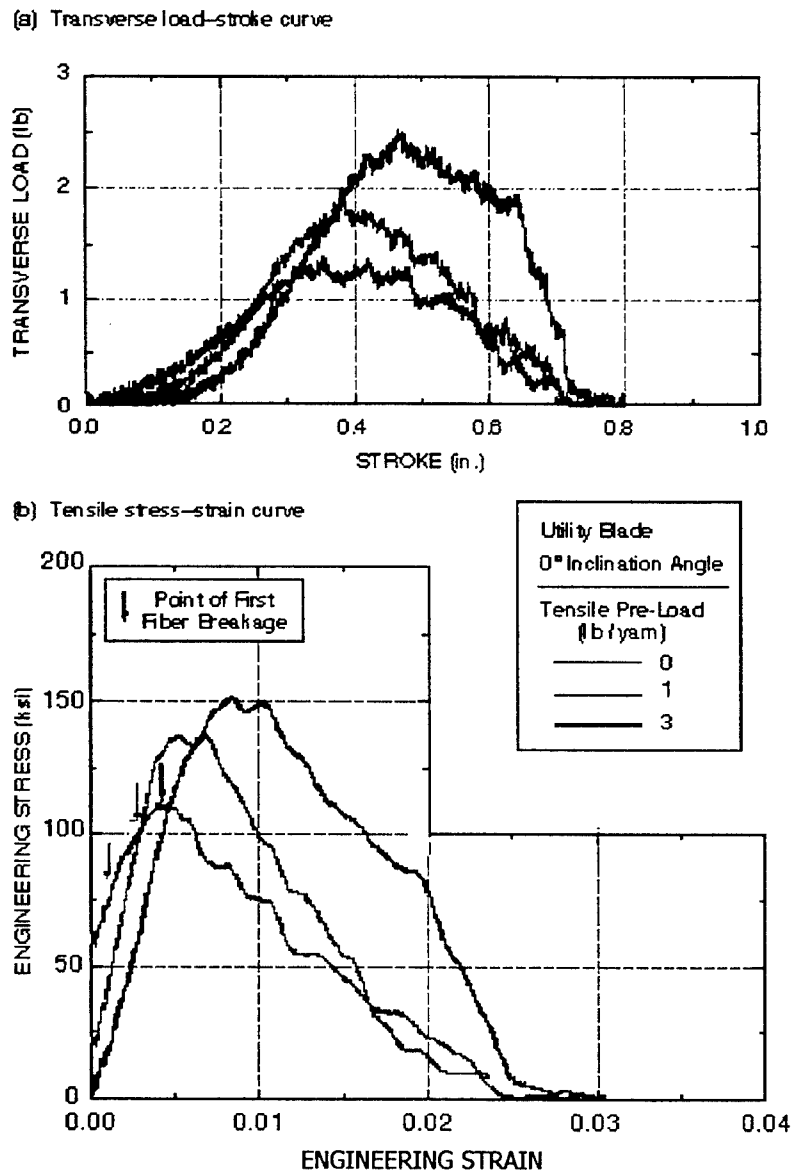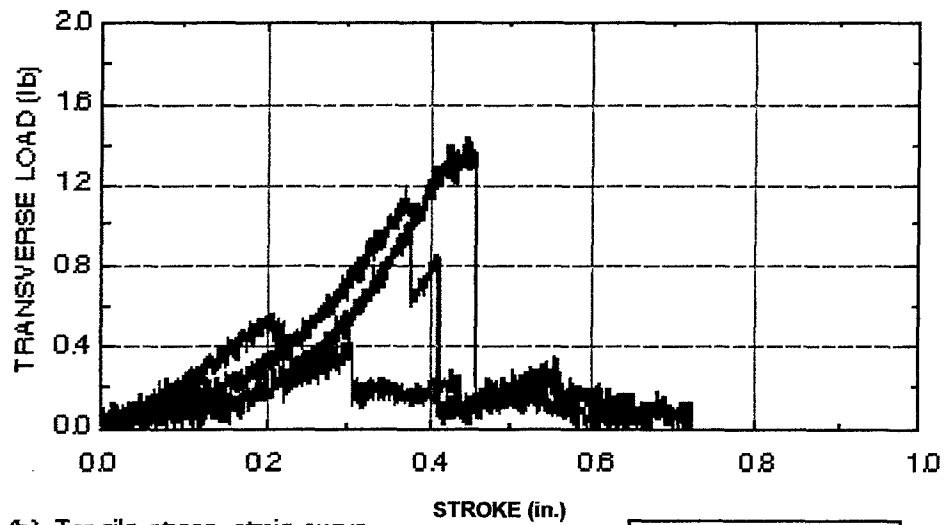

FIGURE A-12. EFFECT OF AXIAL PRE-TENSION ON TRANSVERSE CUT TEST
BEHAVIOR OF ZYLON YARNS

A-16

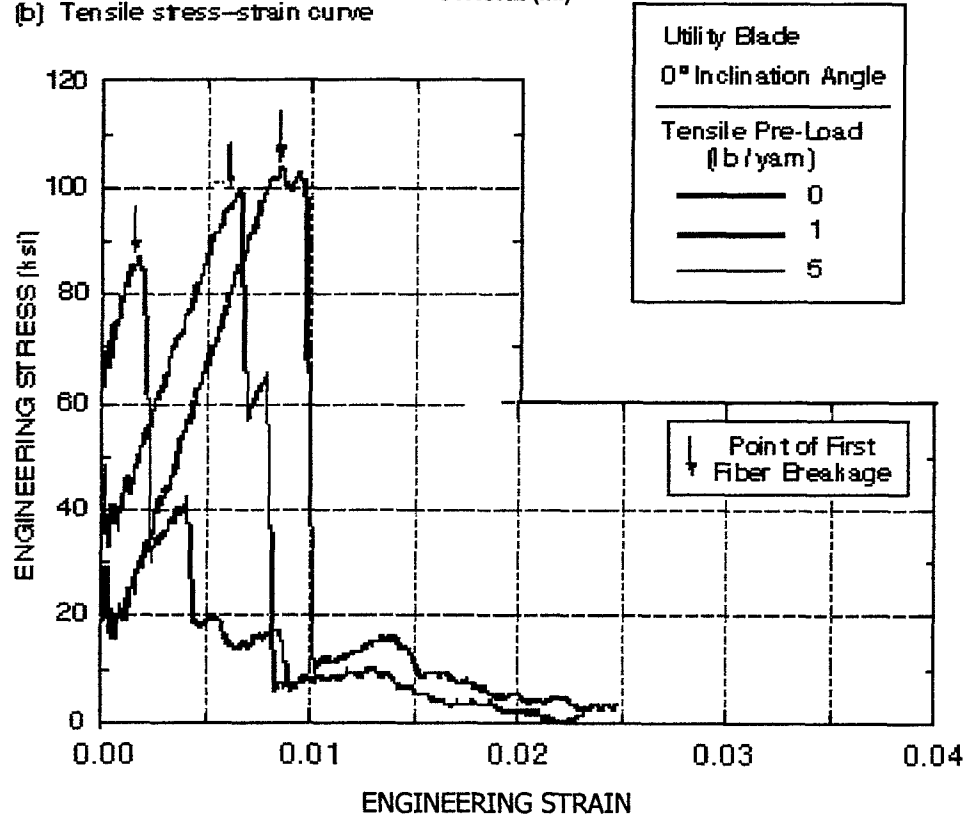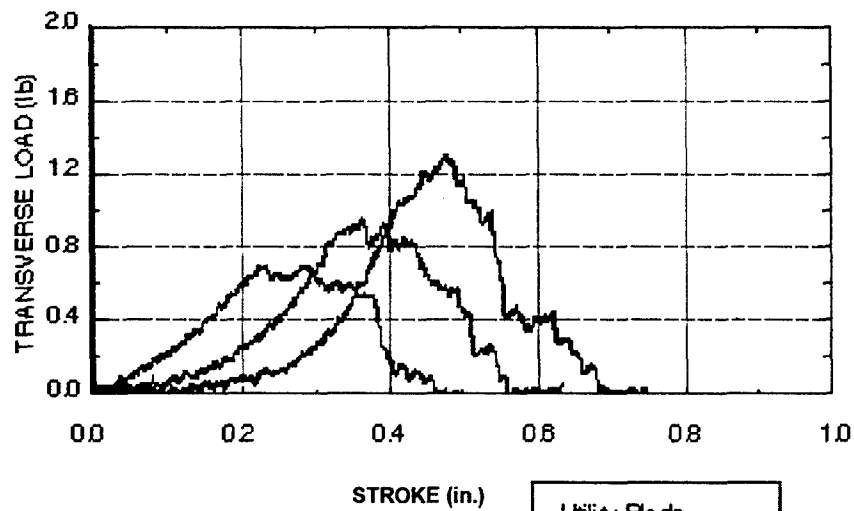(a) Transverse load–stroke curve

(b) Tensile stress–strain curve

FIGURE A-13. EFFECT OF AXIAL PRE-TENSION ON TRANSVERSE CUT TEST
BEHAVIOR OF KEVLAR YARNS

A-17

(a) Transverse load–stroke curve
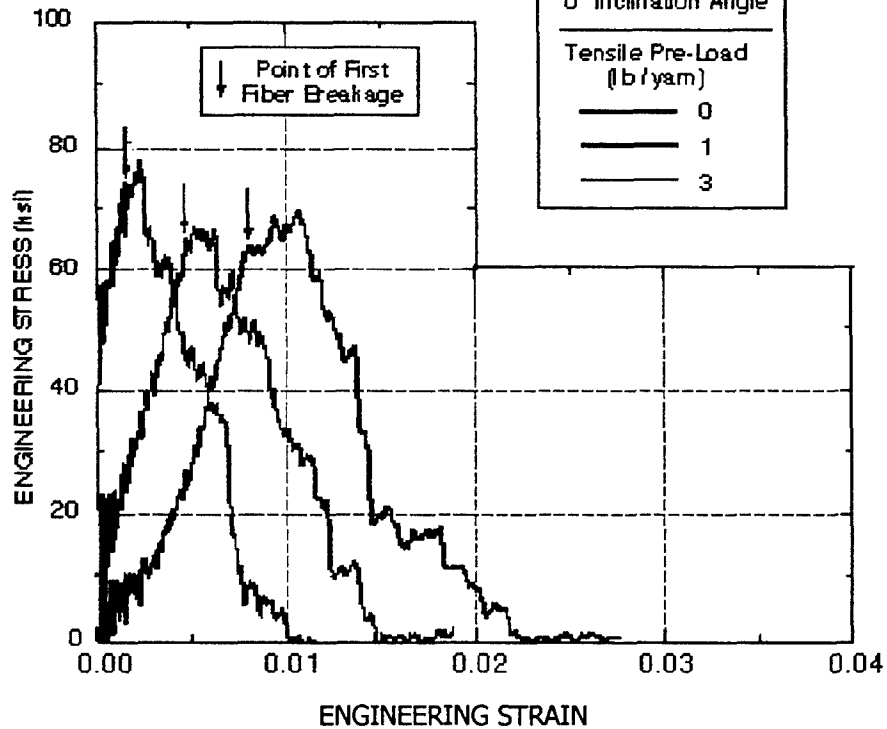
(b) Tensile stress–strain curve

FIGURE A-14. EFFECT OF AXIAL PRE-TENSION ON TRANSVERSE CUT TEST
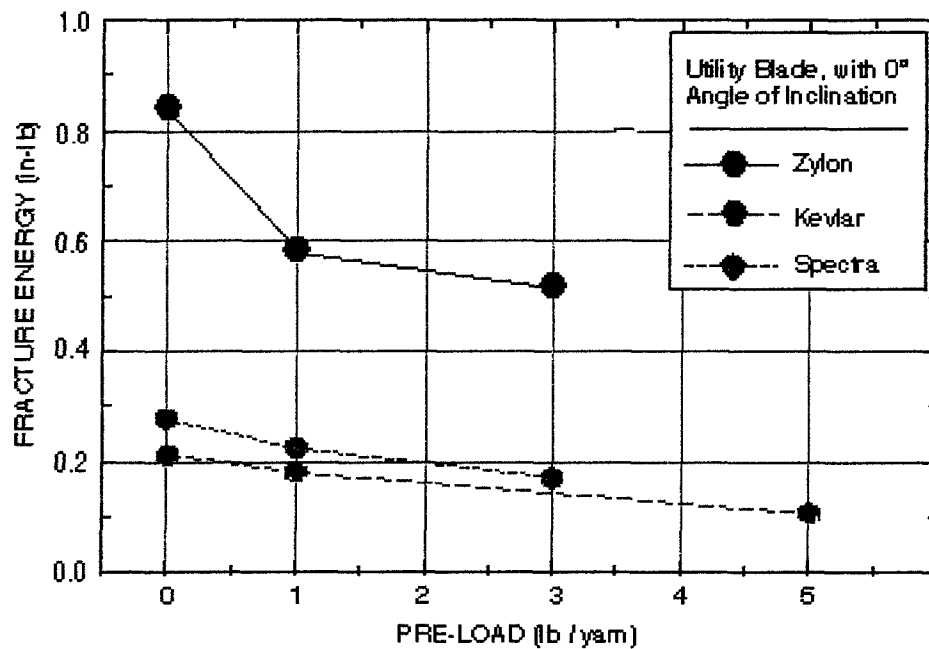BEHAVIOR OF SPECTRA YARNS

FIGURE A-15. DEPENDENCE OF FRACTURE ENERGY UPON TENSILE
PRE-LOAD IN THE TRANSVERSE CUT TESTS

PLANS.

During the next program year, the analysis of the transverse cut resistance tests will be
completed. Scanning Electron Microscope pictures of the ends of cut fibers will be examined to
determine the failure phenomenology and to better understand the fracture energy results
presented above. Fiber tensile failure, indentation failure, and shear failure have been observed.
These failure mechanisms will be related to the materials and test conditions, and to the
measured fracture energies. This analysis will be detailed in the next annual report, as well as in
a journal paper.

REFERENCES.

A-1.   D.A. Shockey, J.H. Giovanola, J.W. Simons, D.C. Erlich, R.W. Klopp, and S.R. Skaggs,
        "Advanced Armor Technology Application Potential for Engine Fragment Barriers for
        Commercial Aircraft," DOT/FAA/AR-97/53, William J. Hughes Technical Center,
        Atlantic City International Airport, New Jersey, July 1997.

A-2.   D.A. Shockey, D.C. Erlich, and J.W. Simons, "Improved Barriers to Turbine Engine
        Fragments, Interim Report III," DOT/FAA/AR-99/8,III, William J. Hughes Technical
        Center, Atlantic City International Airport, New Jersey, May 2001.

A-3.   ASTM-F-1790, "Standard Test Method for Measuring Cut Resistance of Materials Used
        in Protective Clothing," ASTM Committee F 23, Philadelphia, Pennsylvania, 1997.

A-4.   European Committee for Standardization, "Protective Gloves Against Mechanical Risks, Section 6.2 Blade Cut and Section 6.5 Impact Cut" EN 388: 1994, CEN Secretariat, rue de Stassart 36, B-1050 Brussels, Belgium.

A-5.   R.H. Turner and D.M. Smith, "Development of a New Cut Test for Protective Gloves Against Machine-Driven Knives," ASTM STP 1273, pp. 126-139, 1997.

A-6.   J. Lara, D. Turcott, R. Daigle, and J. Boutin, "A New Test Method to Evaluate the Cut Resistance of Glove Materials," ASTM STP 1237, pp. 23-31, 1996.

A-7.   M.C. Boyce, M.L. Palmer, M.H. Seo, P. Schwartz, and S. Backer, "A Model of the Tensile Failure Process in Woven Fabrics," Journal of Applied Polymer Science, Applied Polymer Symposium, Vol. 47, pp. 383-402, 1991.